



# Geochemistry, Geophysics, Geosystems

# RESEARCH ARTICLE

10.1029/2020GC009419

# **Key Points:**

- Shell cleaning preferentially removes inner calcite and favors the low trace element (TE) crust/cortex calcite in two nonspinose species
- Preferential removal of inner calcite biases TEs toward lower values and can be problematic for downcore data interpretation
- Evaluating cleaning methods via high-resolution techniques may increase the utility of Ba/Ca, Mn/Ca, and Zn/Ca in paleo-reconstructions

### **Supporting Information:**

· Supporting Information S1

# Correspondence to:

T. Fritz-Endres, fritzent@oregonstate.edu

### Citation:

Fritz-Endres, T., & Fehrenbacher, J. (2021). Preferential loss of high trace element bearing inner calcite in foraminifera during physical and chemical cleaning. *Geochemistry, Geophysics, Geosystems*, 22, e2020GC009419. https://doi.org/10.1029/2020GC009419

Received 4 SEP 2020 Accepted 7 DEC 2020

# Preferential Loss of High Trace Element Bearing Inner Calcite in Foraminifera During Physical and Chemical Cleaning

Theresa Fritz-Endres<sup>1</sup>, and Jennifer Fehrenbacher<sup>1</sup>

<sup>1</sup>College of Earth, Ocean and Atmospheric Sciences, Oregon State University, Corvallis, OR, USA

**Abstract** Trace elements (TEs) in the calcite shells of foraminifera are widely used in paleoceanographic reconstructions. Nearly all TE analytical protocols include cleaning to remove contaminant phases. Understanding, how the TE composition is altered during physical and chemical cleaning is of utmost importance in ensuring the accuracy of paleoclimate reconstructions. Aggressive cleaning steps that include corrosive reagents are commonly used to clean shells with elevated Ba/Ca and Mn/Ca ratios, under the assumption that these elements are elevated due to diagenetic overprinting. We provide evidence that elevated intrashell Ba/Ca, Mn/Ca, and Zn/Ca ratios are lattice bound and a primary signal incorporated into inner calcite during calcification in the nonspinose species Neogloboquadrina dutertrei and Pulleniatina obliquiloculata. We first demonstrate, using laser ablation depth profiling analyses, that aggressive cleaning following the full cleaning protocol traditionally used to eliminate Mn and Ba contamination, preferentially removes inner (ontogenic) calcite and favors the low Ba/Ca, Mn/ Ca, Zn/Ca, and Mg/Ca crust/cortex calcite. In a separate experiment, we demonstrate that mechanical fragmentation of bulk shells prepared for solution analysis also preferentially removes inner calcite and favors the low TE crust/cortex calcite. Preferential loss of the ontogenic calcite decreases Ba/Ca, Mn/ Ca, and Zn/Ca ratios by 50%-90% in N. dutertrei and P. obliquiloculata shells. This biases foraminiferal TE results toward lower values and may yield data that is problematic for the interpretation of downcore records.

Plain Language Summary Elements (including barium and magnesium) measured inside microscopic fossil shells are higher than expected and could reflect contamination or could reflect key information about the ancient surface ocean. For example, barium may reflect how much organic carbon is produced in the surface ocean, some of which is sunk to the deep ocean and thus removed from exchange with the atmosphere, effecting climate. Previous studies have attributed higher concentrations of these elements to contamination that forms on shells and have established harsh chemical cleaning techniques to remove the contamination. However, these cleaning techniques also remove parts of the shell that contain key information about past ocean conditions. We determine that high concentrations of these elements are not due to contamination in our samples and likely reflect conditions of the surface ocean. In future work, we suggest using techniques that measure at the microscale to confirm that there is no contamination and we suggest using more careful cleaning that preserves these elements. Preserving these elements in fossil shells may provide key information about organic carbon production and cycling in the surface ocean, which is critical to reconstruct carbon exchange between the atmosphere and ocean.

# 1. Introduction

The geochemistry of planktic foraminifera shells is a critical tool used to reconstruct paleotemperature (Mg/Ca; Anand et al., 2003; Dekens et al., 2002; D. W. Lea et al., 1999; von Langen et al., 2005), redox conditions (Mn/Ca; Glock et al., 2012; Groeneveld et al., 2018; Klinkhammer et al., 2009; Petersen et al., 2019; Skinner et al., 2019), freshwater flux and salinity (Ba/Ca; Bahr et al., 2013; Evans et al., 2015; Hall & Chan, 2004; Hoffmann et al., 2014; Setiawan et al., 2017; Weldeab et al., 2007a; 2014), and nutrients (Mn/Ca; Zn/Ca; Ba/Ca; Marr et al., 2013) in ancient water masses. Together, mixed layer dwelling and deeper dwelling planktic foraminifera species allow for reconstructions of the entire upper water column (e.g., Chaisson & Ravelo, 2000; Mulitza et al. 1997; Spero et al., 2003).

© 2020. American Geophysical Union. All Rights Reserved.



Trace element (TE) to Ca ratios, including Ba/Ca, Mn/Ca, and Zn/Ca, in many nonspinose deeper dwelling foraminifer species are higher and Ba/Ca, Mn/Ca, Zn/Ca, and Mg/Ca are more variable as compared to mixed layer dwelling foraminifera, and their utility in paleoceanographic reconstructions is less straight-forward (Branson et al., 2015; Fehrenbacher & Martin, 2010; Hathorne et al., 2009; Jonkers et al., 2012, 2016; Kunioka et al., 2006; A. Y. Sadekov et al., 2005). Often, the TEs in nonspinose foraminifer shells are elevated in the ontogenic calcite with distinct high and low TE bands and TEs are low and relatively invariable within the outer crust or cortex of the shell (Eggins et al., 2003; Hathorne et al., 2009; Steinhardt et al., 2015). High intrashell TE/Ca bands are often correlated in nonspinose foraminifera (Eggins et al., 2003; Hathorne et al., 2009), suggesting similar environmental or biological control on the incorporation of these TEs. High TE/Ca bands may reflect the environmental conditions at the time of calcification. For example, high Mn/ Ca and Zn/Ca ratios in foraminiferal calcite are thought to reflect increasing concentrations of these metals from low values in surface waters to higher values at depth and may be used to trace surface waters and nutrient stratification (Boyle, 1981; Marr et al., 2013). While few studies have been done evaluating Zn/Ca in planktic foraminifera, Zn/Ca ratios in benthic foraminifera may be used with other TE/Ca ratios to trace changes in deep water carbonate chemistry (Marchitto et al., 2000) and, in shallow water cores, changes in the nutricline (Bryan & Marchitto, 2010). Dissolved Mn is additionally modified by redox conditions and high Mn/Ca ratios in benthic foraminifera have been used to reflect oxygenation of hypoxic deep water and pore water (Glock et al., 2012; Groeneveld et al., 2018; Petersen et al., 2019; Skinner et al., 2019). In regions with intense oxygen minimum zones, comparing the Mn/Ca ratio of species of planktic foraminifera that calcified in the mixed layer to those that calcified in the thermocline and to benthic foraminifera may be used as a proxy for changing terrestrial input of Mn and oxidation reduction reactions in the water column (Klinkhammer et al., 2009) and Mn/Ca in sediment trap derived planktic foraminifera may in part reflect changing conditions within an oxygen minimum zone (Davis et al., 2020).

High Ba/Ca ratios in surface dwelling foraminifera reflect changes in freshwater flux and salinity in regions with high freshwater input (Bahr et al., 2013; Edmond et al., 1978; Evans et al., 2015; Weldeab et al., 2007b, 2014). High Ba/Ca ratios in nonspinose deeper dwelling foraminifera may in part reflect higher Ba concentrations in deeper water; however, Ba/Ca ratios are often much higher than in surface dwelling species and higher than can be attributed to the Ba composition of any seawater location (Bahr et al., 2013; Hall & Chan, 2004; Hathorne et al., 2009; Lea & Boyle, 1991). High Ba/Ca ratios measured in *Neogloboquadrina dutertrei*, and likely in other nonspinose foraminifera, may reflect conditions within a Ba enriched microenvironment, such as within marine snow particulates or other organic detritus in the water column (Fehrenbacher et al., 2018; Greco et al., 2019; Takagi et al., 2019). Within particles, the desorption of Ba from Fe hydroxides and the degradation of organic matter can enrich Ba and SO<sub>4</sub> enough to support Ba supersaturation and the formation of barium enriched amorphous particles and barite crystals (BaSO<sub>4</sub>; Martinez-Ruiz et al., 2018; Stroobants et al., 1991; Sternberg et al., 2005), despite widespread barite undersaturation in seawater (Monnin et al., 1999; Rushdi et al., 2000). The complicated geochemistry of particulates may also permit higher dissolved Mn within the particulate microhabitat (due to lower oxygen and pH; Alldredge, 2000; Alldredge & Cohen, 1987), which may help to explain the elevated and variable Mn in nonspinose foraminifers.

Elevated Ba/Ca and Mn/Ca ratios in foraminiferal calcite have also been attributed to contaminants or diagenetic alteration in the water column or on the seafloor (Boyle, 1981, 1983; Boyle & Keigwin, 1985; Gibson et al., 2016; Haley & Klinkhammer, 2002; Lea & Boyle, 1991; Pena et al., 2005, 2008). Although Ba is thought to substitute in place of Ca in inorganic calcite (Kitano et al., 1971) and inside the lattice of a foraminifera shell (Lea & Boyle, 1991; Lea & Spero, 1994), Ba-rich sediment phases can result in nonlattice bound Ba enrichment on shell surfaces and within pores that masks shell bound Ba. Such sediment phases, including Ba-enriched detrital and fine-grained material, barite crystals, organic matter, and Mg-Mn and Fe oxide overgrowths, have been observed associated with foraminifer shells (Gibson et al., 2016; Pena et al., 2005, 2008). Mn-carbonate phases can precipitate under conditions where Mn is remobilized from oxidized organic matter (Boyle, 1983; Pedersen & Price, 1982) and may contaminate the Mn and Mg signal on foraminifera shell surfaces in the water column (Davis & Benitez-Nelson, 2020; Gibson et al., 2016) or on the seafloor (Boyle, 1981; Branson et al., 2015; Pena et al., 2008, 2005). Contamination may also occur during chemical cleaning, as high TE values have also been attributed to TE reabsorption onto cleaned calcite prepared for solution analysis (Haley & Klinkhammer, 2002; Sholkovitz, 1989) such that contaminants cleaned away may still be erroneously measured as a primary signal. Aggressive cleaning procedures (including a



Table 1 Definition of inner versus outer calcite after the definitions of Brown and Elderfield (1996)							
Calcite type	Description						
Inner calcite	Defines all chambers inside the shell as well as calcite of the inner part of the exterior shell wall						
Outer calcite	The outer part of the exterior shell wall that covers inner calcite layers. In the case of <i>N. dutertrei</i> and <i>P. obliquiloculata</i> , the outer calcite includes the crust/cortex calcite						
Cortex calcite	The smooth microperforate veneer that covers P. obliquiloculata inner calcite						
Crust calcite	Calcite layer that forms over inner calcite comprised of large blocky prismatic crystals that often cover inner calcite pore spaces						

reductive cleaning step and the use of the chelating agent diethylene-triamine pentaacetic acid (DTPA)) are traditionally employed to remove contaminant phases (e.g., Lea & Boyle, 1991). These procedures are highly corrosive to calcite, can lead to extensive sample loss due to dissolution, and may decrease TE concentrations (Barker et al., 2003; Johnstone et al., 2016; Martin & Lea, 2002; Lea & Boyle, 1991; Regenberg et al., 2006; Rosenthal et al., 2004; Vetter et al., 2013; Yu et al., 2007). For this reason, the reductive and DTPA steps are often excluded unless metal contaminant phases are observed or suspected (Johnstone et al., 2016; Yu et al., 2007), such as within redox sensitive basins (Pena et al., 2005; 2008).

In this study, we use laser ablation Inductively Coupled Plasma Mass Spectrometry (ICP-MS) to investigate how cleaning procedures alter the TE composition of the nonspinose planktic foraminifer species N. dutertrei and Pulleniatina obliquiloculata. These species were chosen because studies have shown that the TE composition of the inner (ontogenic) calcite in these species is markedly higher than the outer calcite (Eggins et al., 2003; Fehrenbacher et al., 2018; Fehrenbacher & Martin, 2010; Jonkers et al., 2012; Kunioka et al., 2006; A.Y Sadekov et al., 2005, 2009) and the inner calcite of these species is more prone to dissolution on the seafloor (e.g., Johnstone et al., 2010), potentially altering TE concentrations. Laser ablation ICP-MS is an excellent tool for assessing intrashell TE variability (Eggins et al., 2003; Fehrenbacher et al., 2015; Hathorne et al., 2009, 2003; A. Sadekov et al., 2009; Wit et al., 2010). It is minimally destructive to the shell and permits repeat analyses of each specimen before and between each cleaning step, allowing for a detailed assessment of how each cleaning step alters the TE composition. After each cleaning step, we measure intrashell TE/Ca ratios of whole shells and shell fragments using low energy and low repetition rate laser settings, enabling us to resolve "inner" versus "outer" calcite (as defined in Table 1) and corresponding TE/Ca variability within the shell. In addition to the laser analyses, we also investigate how bulk (solution) cleaning methods alter the trace element composition of P. obliquiloculata. We use Scanning Electron Microscope (SEM) imaging to investigate how bulk cleaning modifies shell fragments. We find that the aggressive cleaning steps often employed to remove contaminant phases also decrease or completely remove inner calcite in N. dutertrei and P. obliquiloculata and decrease the mean TE composition.

# 2. Methods

# 2.1. Individual Shell Laser Ablation ICP-MS

Specimens of *N. dutertrei* and *P. obliquiloculata* were obtained from the 355–500 µm size fraction of the 7–80 cm interval of Eastern Equatorial Pacific (EEP) core ME0005A-43JC (7.86°N, 83.6°W, and water depth 1,368 m). This interval was chosen because preliminary laser ablation data indicate that *N. dutertrei* and *P. obliquiloculata* shells have high Ba/Ca and Mn/Ca ratios and specimens display intrashell TE banding (Figure S1). Four *N. dutertrei* and one *P. obliquiloculata* were left whole and 14 *N. dutertrei* and 15 *P. obliquiloculata* were placed on a rubber stopper, wetted, and gently broken with a scalpel into four to five large fragments.

The whole shells and fragments were cleaned using the established cleaning procedures of Martin and Lea (2002), adapted for single shells (see Appendix A), and included the Cd-cleaning step employed by Boyle and Keigwin (1985) and Lea and Boyle (1989) and others (e.g., Lea & Boyle, 1991). The cleaning steps included rinses to remove finely adhering clays, an oxidative step to remove remnant organic matter, the reductive step to remove metal oxides, and finally, the DTPA step that is typically only used in settings where



contaminant surface phases are problematic. Briefly, shell material was rinsed in methanol and sonicated (10 s) followed by four ultrapure water (18 M $\Omega$ ) rinses. Rinses were followed by an oxidative cleaning step in which shells were bathed for 10 min in a warm (60°C) buffered hydrogen peroxide solution followed by four ultrapure water rinses. Shell material was then reductively cleaned with an anhydrous hydrazine/ammonium citrate solution warmed to 80–90°C for 30 min followed by four ultrapure water rinses. Shell material underwent a final cleaning with an alkaline chelating agent of weak (0.002 M) DTPA solution buffered in 0.05 M NaOH warmed to 100°C for 5 min. DTPA was then neutralized by additions of 0.01 M NaOH followed by rinsing shell material three times with ultrapure water. During the final rinse step, the foraminifers were bathed for 30 min at 100°C. The final step was followed by a dilute acid (0.001 M HNO<sub>3</sub>) leach to remove any adsorbed contaminants from the shell material followed by ultrasonication and a final ultrapure water rinse. In between each cleaning step (rinses/sonication, oxidative, reductive, and DTPA + acid leach), the whole shells and fragments were mounted onto aluminum stubs with carbon tape, analyzed on a laser, and imaged on an SEM.

Laser ablation depth profile analyses were conducted at Oregon State University (OSU) using a Teledyne/ Photon Machines 193 nm ArF UV excimer laser ablation system with a HelEx laser ablation cell coupled to a Thermo Scientific X-series II quadrupole ICP-MS. Gas composition and flow rate were determined by adjusting the flow of Ar and He as necessary to achieve high count rates on the sample/standard while maintaining  $ThO^+/Th^+$  ratios less than 0.4% (tuned daily). Whole shells were analyzed from the outside-in and shell fragments were analyzed from the inside-out. Samples were analyzed using a 50–70  $\mu$ m diameter spot size at 4 Hz repetition rate and 1.0–1.5  $J/cm^2$  laser fluence. Data acquisition varied between 40 and 60 s per spot analysis. Repeat analyses were conducted on chambers large enough to permit multiple spots. Isotopes, including  $^{137}$ Ba,  $^{24}$ Mg,  $^{25}$ Mg,  $^{43}$ Ca,  $^{44}$ Ca,  $^{66}$ Zn,  $^{88}$ Sr,  $^{27}$ Al, and  $^{55}$ Mn, were measured along with others not assessed in this study.  $^{43}$ Ca was used as the internal standard and  $^{44}$ Ca was monitored for consistency.

Shell profile mean elemental concentrations were calculated using LAtools data reduction software that includes screening for outliers and background correcting by subtracting average background counts (calculated with the laser off) from each data point (Branson et al., 2019). The mean TE/Ca ratio for each profile was then calculated by normalizing to the known TE concentration in the drift/background-corrected bracketed analyses of the NIST SRM 610 and 612 glass standards at 5 Hz and  $\sim 4.5$  J/cm² laser fluence (Jochum et al., 2011). Ten repeat analyses gave a reproducibility of the mean Ba/Ca, Mn/Ca, Zn/Ca, and Mg/Ca ratios of 1,594  $\pm$  69  $\mu$ mol/mol ( $\pm$ 4.3%; 1 $\sigma$ ), 3,885  $\pm$  75  $\mu$ mol/mol ( $\pm$ 1.9%; 1 $\sigma$ ), 3,446  $\pm$  89  $\mu$ mol/mol ( $\pm$ 2.6%; 1 $\sigma$ ), and 9.655  $\pm$  0.49 mmol/mol ( $\pm$ 5.0%; 1 $\sigma$ ), respectively, for NIST 610 and 139  $\pm$  5.0  $\mu$ mol/mol ( $\pm$ 3.7%; 1 $\sigma$ ), 331  $\pm$  14  $\mu$ mol/mol ( $\pm$ 4.1%; 1 $\sigma$ ), 296  $\pm$  14  $\mu$ mol/mol ( $\pm$ 4.6%; 1 $\sigma$ ), and 1.289  $\pm$  0.90 mmol/mol ( $\pm$ 7.0%; 1 $\sigma$ ), respectively for NIST 612. Standard measurements are within 5.0% of published values for NIST 610 and 612 (Jochum et al., 2011).

After each laser ablation session, the whole shell and shell fragments were imaged on a Quanta 300 environmental SEM at OSU. Thickness was measured from profile images of each shell fragment and used to convert ablation time to distance ( $\mu m$ ). The SEM images were used to visually assess the effect of cleaning on shell material and microstructure changes. Because shell fragments were fragile and easily lost, SEM analysis was skipped after the oxidative step and only done after the reductive step to reduce the number of times fragments were removed from and remounted on the tape. Thus, the images taken after reductive cleaning represent impacts to the shell material that occurred during both the oxidative and reductive cleaning.

# 2.2. Bulk Shells Prepared for Solution Analysis

The purpose of the bulk shell cleaning study is to assess the effect of sample cleaning on shell TE/Ca ratios. Specifically, we modify the shell cracking procedure and use two different settling times before aspirating the rinse/cleaning solutions. We then assess shell fragmentation using image analysis. Forty *P. obliquiloculata* shells were selected from the 8 to 10 cm (Holocene) and 40 from the 26 to 28 cm (deglacial) intervals from western equatorial Pacific core MW91-9-6GGC (2.02°S, 156.93°E, water depth 1,625 m). Shells were grouped into sets of 20 and gently cracked between two glass slides to open chambers to aid the removal of clays and other debris. Shell fragments were homogenized with a brush and were split into two aliquots for a total of 16 bulk groups (eight replicates from each interval). Four groups for each interval were subjected to the Mg-only cleaning protocol (Barker et al., 2003), which included rinses/sonication, oxidative cleaning,



and a weak (0.001 M) HNO<sub>3</sub> leach and a 1 min settling time before aspirating the rinse/cleaning solution. Four groups from each interval were cracked open more gently and the settling time before aspirating the rinse/cleaning solution was increased from 1 min to 3 min.

Prior to cleaning, shell fragments were imaged on a dark background at 0.8 and  $10.0 \times z$  zoom using a Leica M125 stereomicroscope with a DMC 4500 mounted camera system. Images were processed using Fiji software package (Schindelin et al., 2012) to analyze and categorize shell fragments as shown in Figure S2. Two images of each group were used for each image analyses. Shell fragments were distinguished from background using the Auto Threshold v1.17 Fiji plugin. Shell fragment surface area was calculated using the Analyze Particles tool and categorized as either large (>6  $\mu$ m²) or small fragments (<6  $\mu$ m²) for each sample (changing the categorization by  $\pm$  3  $\mu$ m² changes the number of large or small fragments by < 5%).

Following cleaning, fragments were carefully mounted on their longest axis onto aluminum stubs with carbon tape and analyzed on a FEI Quanta 600F environmental SEM at OSU. Each sample was imaged at higher and lower magnification (horizontal field width  $\sim$ 1 mm and  $\sim$ 500  $\mu$ m). Regions of shell fragments were visually interpreted as either "inner" or "outer" calcite (as defined in Table 1). The outer calcite of P. obliquiloculata is dominated by a shell cortex that is characterized by a smooth microperforate texture. The cortex is identifiable as a thin and finely crystalline layer that appears glassy under SEM (Johnstone et al., 2010), while the inner calcite can be thicker and coarsely crystalline and is identifiable by larger uniformly spaced pores and high ridges between pore spaces. The visual categorization of inner and outer calcite at higher magnification (~1 mm horizontal field width) was used to train Weka Trainable Segmentation (v.3.2.33), a Fiji plugin with machine learning techniques (Figure S2). Using Weka Trainable Segmentation, machine learning algorithms classified each image pixel to a class (inner or outer calcite) for all SEM images and calculated the total inner calcite and outer calcite surface area present in each replicate. Inner calcite has a distinct SEM grayscale range compared to outer calcite (8-bit grayscale range 100-210 and 210-255, for the inner and the outer calcite, respectively) as a result of the very different pore structure (e.g., microperforate outer calcite has lighter grayscale values), allowing for an accurate classification (using standard Weka settings, out-of-bag error for a well-trained run was typically < 1%).

# 3. Results

# 3.1. Individual Shells

# 3.1.1. Visual Changes in Shell Texture

SEM images of whole shell and shell fragments of N. dutertrei and P. obliquiloculata material taken after each cleaning step indicate progressive dissolution during cleaning with preferential loss of inner portions of the shell (Figure 1; microstructure descriptions based on those presented in Dittert and Henrich [2000] and Regenberg et al. [2013]). After the initial rinses/sonication, all N. dutertrei fragments and whole shells appear well preserved. SEM images reveal regularly spaced outer pores surrounded by irregular ridges, preserved shell layers, smooth interpore areas, round to funneled pores, high to slightly reduced ridges, thick outer calcite, and sharp edges of euhedral crystal structures (Figures 1a and 1b). After the oxidative and reductive steps (to preserve fragile shell fragments, SEM analysis was skipped after the oxidative step and only done after the reductive step), N. dutertrei material show signs of dissolution with cracked and disintegrated inner calcite layers, funneled pores (Figures 1c and 1d), and slightly rounded crystal surfaces on the exterior of the shell (Figure 1d). After the DTPA step, N. dutertrei material show signs of substantial dissolution (Figures 1e and 1f). The inner calcite appears heavily dissolved and calcite of the inner chamber wall is eroded, and the exterior calcite crystals are heavily dissolved and rounded (Figure 1f). SEM images of P. obliquiloculata taken after the initial rinses/sonication reveal smooth outer calcite, intact calcite layers, smooth inner calcite with round to funneled and evenly spaced pores and smooth interpore areas (Figures 1g and 1h). Often in cracking open P. obliquiloculata shells, inner calcite layers delaminate from outer calcite and are sheeted away in one or many distinct layers (Figure 1j). Delamination occurs in a few fragments after just the initial rinses/sonication and before more corrosive cleaning steps are conducted. After oxidative and reductive cleaning, the inner calcite separated from the cortex in two of 15 fragments (Figure 1j) and in another two fragments, the inner calcite is completely missing and just the cortex remains. After DTPA cleaning,

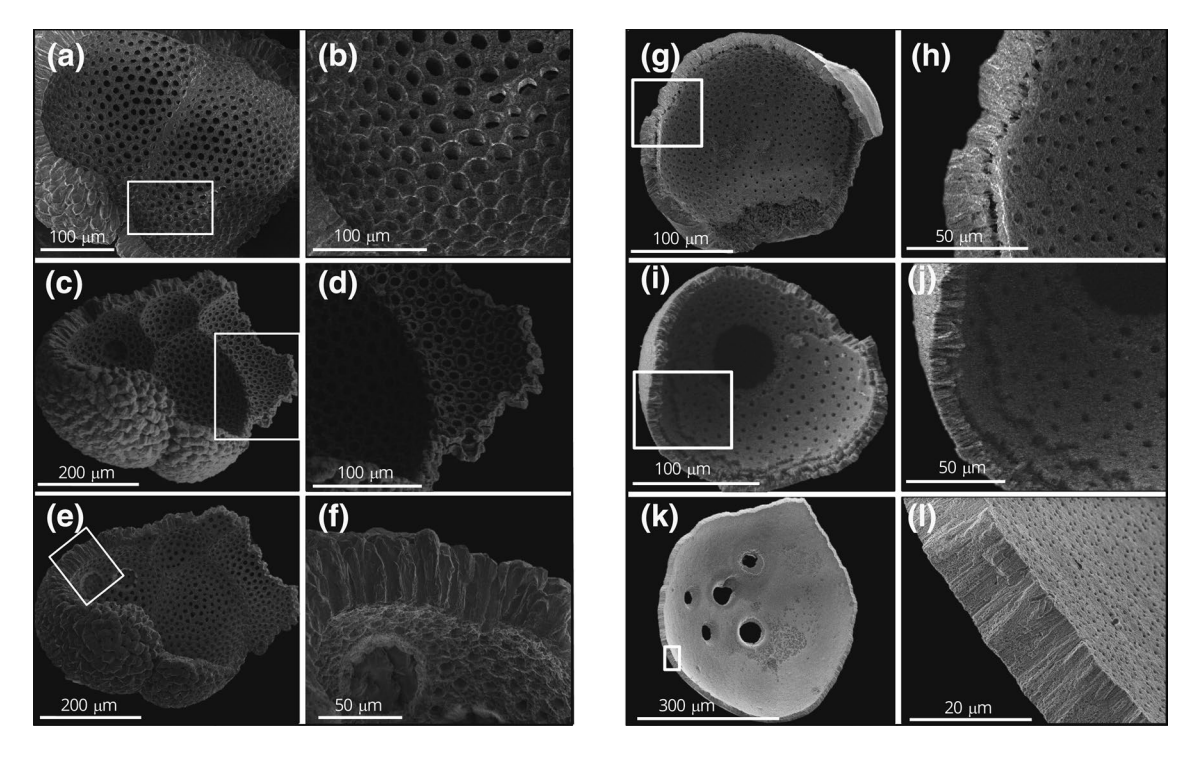


**Figure 1.** Scanning electron micrograph (SEM) images of examples of *N. dutertrei* (a–f) and P. obliquiloculata (g–l) shells that show progressive dissolution from initial rinses (a and g), to oxidative and reductive cleaning (c and i), and DTPA cleaning (e and k). White boxes show the area that is magnified in the corresponding panel. DTPA, diethylene-triamine pentaacetic acid.

*P. obliquiloculata* material shows clear divisions between cortex and inner calcite and show separation and removal of portions of inner calcite layers, severely cracked inner calcite, and heavily funneled pores. For three of the shell fragments, inner calcite is completely absent after the DTPA step (Figures 1k and 1i).

# 3.1.2. Laser Ablation Results

# 3.1.2.1. Depth profiles after initial rinse/sonication

Laser ablation profiles of samples that have undergone just initial rinses contain high and variable TEs (Figures 2 and 3). Laser ablation profiles of nearly all (90%, N=16) of N. dutertrei shells have distinct regions of high TEs within the inner calcite (e.g., Figure 2, blue lines). These regions are  $10-30~\mu m$  thick and have two to four alternating high/low TE/Ca bands. Bands of high Mn/Ca, Zn/Ca, and Mg/Ca are variable from specimen-to-specimen and less reproducible from chamber-to-chamber than bands of high Ba/Ca. TE bands are often, but not always, correlated (e.g., Figures 2a vs. 2b). Most (80%, N=13) of P. obliquiloculata shells have alternating bands of high and low TE in inner calcite, like those observed in N. dutertrei, although there are fewer bands (one to two) and they are more variable from chamber-to-chamber (e.g., Figure 3, blue lines). All profiles of N. dutertrei and P. obliquiloculata have a low and homogenous TE region on the outside that is  $10-20~\mu m$  thick and likely represents crust/cortex calcite, which has been shown in other laser ablation studies with this species to have homogeneous trace element (TE) ratios (e.g., Jonkers et al., 2012; Sadekov et al., 2009; Steinhardt et al., 2015).

The regions of high TE outer calcite is differentiated from low TE inner calcite at the point of greatest change in Ba/Ca, Mn/Ca, Zn/Ca, and Mg/Ca ratios from high and variable values to low and homogenous values (Figure 4). In *N. dutertrei*, 65% of the total calcite is high TE calcite, on average, and *P. obliquiloculata* contains 55% high TE calcite. This is consistent with other studies of *N. dutertrei* (Jonkers et al., 2012) and *P. obliquiloculata* (Sadekov et al., 2009; Steinhardt et al., 2015) and the low TE regions in *P. obliquiloculata* correspond with the smooth micro-perforate cortex observed in SEM images. In both *N. dutertrei* and *P.* 



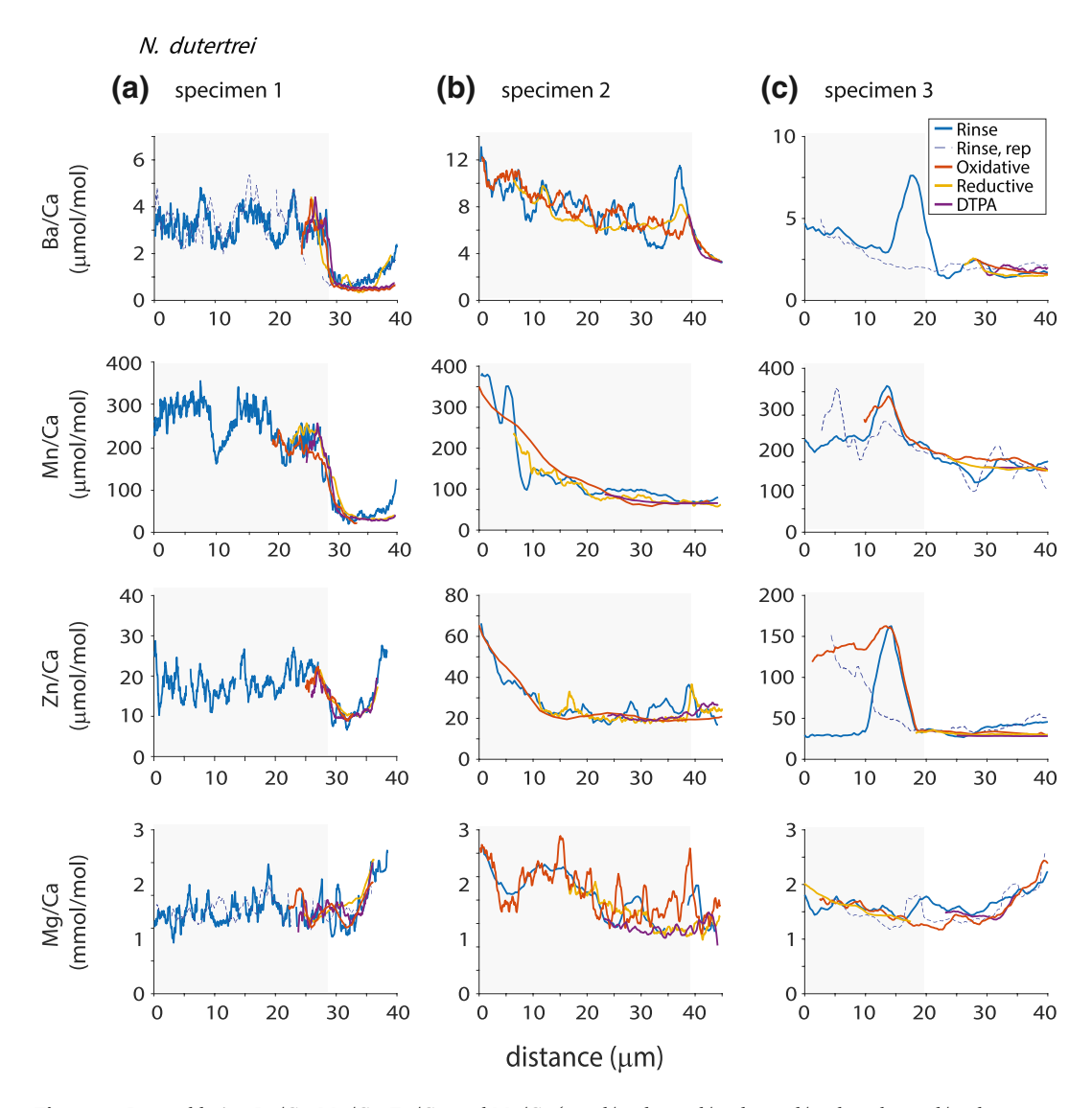


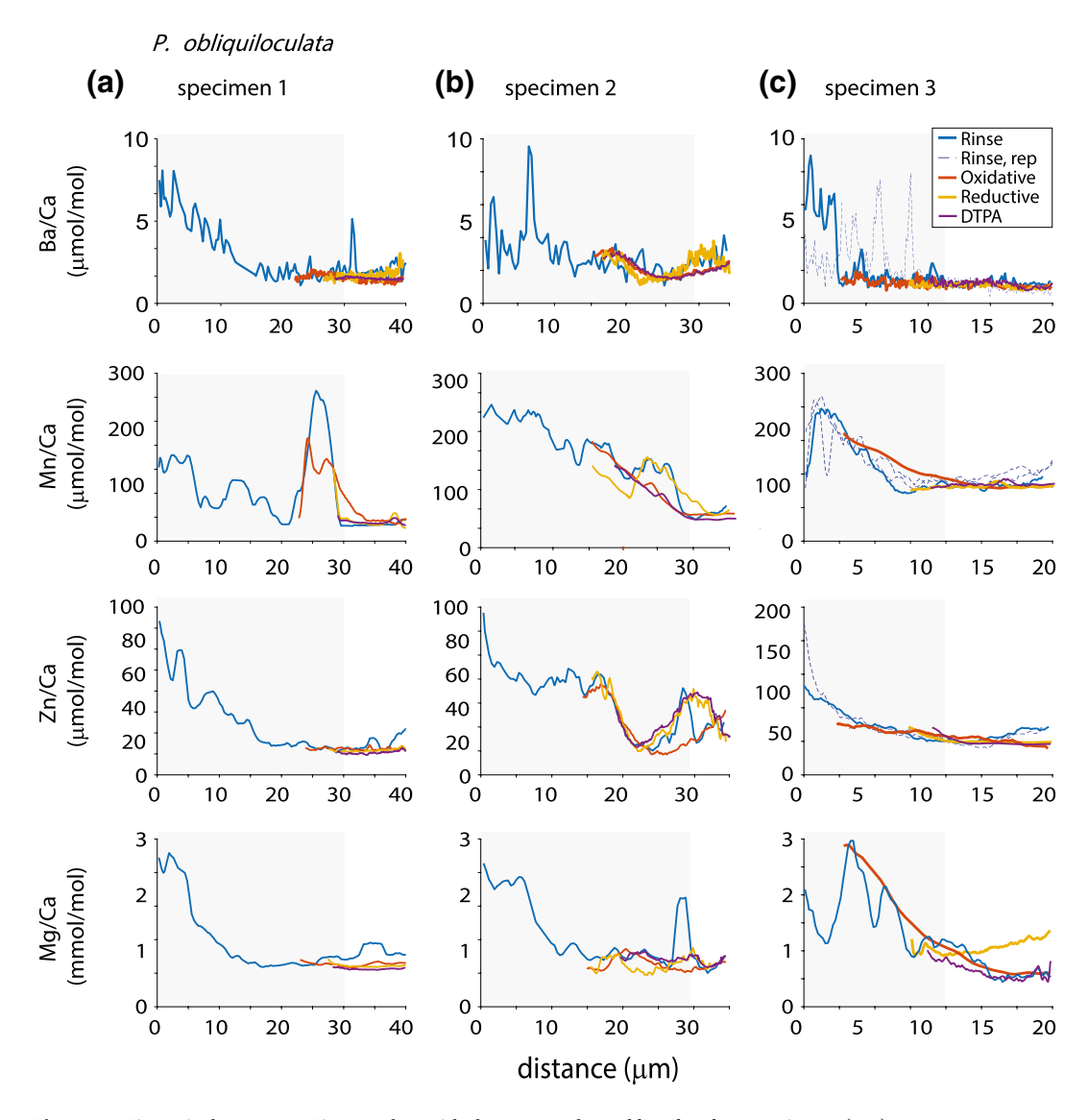
Figure 2. Laser ablation Ba/Ca, Mn/Ca, Zn/Ca, and Mg/Ca ( $\mu$ mol/mol,  $\mu$ mol/mol,  $\mu$ mol/mol, and mmol/mol, respectively) profiles of three example *N. dutertrei* specimens (a-c) subject to initial rinses/sonication (blue line, repeat analysis performed on some shells is shown as blue dashed line), oxidative cleaning (orange line), reductive cleaning (yellow line), and a DTPA + acid leach (purple line). High trace element inner calcite is indicated with a gray box. DTPA, diethylene-triamine pentaacetic acid.

obliquiloculata, inner calcite Ba/Ca, Mn/Ca, and Zn/Ca ratios are 60%–80% higher than the outer (low TE) calcite and have 40%–90% greater variability ( $1\sigma$ ; Table 2). Mg/Ca ratios in the inner calcite are 30%–40% higher than the outer (low TE) regions.

# 3.1.2.2. Oxidative cleaning

After the oxidative cleaning step, *N. dutertrei* shell thickness decreased by an average of 15% and one or more high TE bands are removed (e.g., Figure 2, orange lines). TE/Ca ratios decrease by 40%, 8%, 24%, and 20% for Ba/Ca, Mn/Ca, Zn/Ca, and Mg/Ca ratios, respectively (Figure 5). The decrease in Ba/Ca and Zn/Ca is significant (Student's *t*-test, two-tailed, p < 0.05), while Mn/Ca and Mg/Ca ratios are not significantly different (Student's *t*-test, two-tailed, p = 0.08, and 0.16, respectively).

*Pulleniatina obliquiloculata* shell thickness decreased by an average of 10% and inner calcite is preferentially removed (e.g., Figure 3, orange lines). TE/Ca ratios decrease by 51%, 50%, 59%, and 24% for Ba/Ca, Mn/Ca, Zn/Ca, and Mg/Ca ratios, respectively. The decrease in all Ba/Ca, Mn/Ca, and Zn/Ca ratios are



 $\textbf{Figure 3.} \ \ \text{Figure is the same as Figure 2, but with three example \textit{P. obliquiloculata} specimens (a-c).}$ 

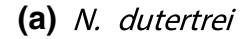
statistically significant (Student's t-test, two-tailed, p < 0.05), while the decrease is not significantly difference for Mg/Ca ratios (Student's t-test, two-tailed, p = 0.22).

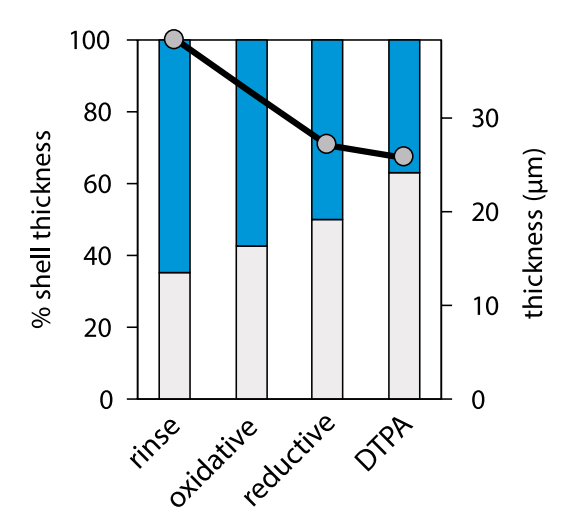
# 3.1.2.3. Reductive cleaning

After the reductive step, N. dutertrei shell thickness decreased by an average of 30% and few high TE/Ca bands remain (e.g., Figure 2, yellow lines). Ba/Ca, Mn/Ca, and Zn/Ca ratios decrease by 75%, 41%, and 89%, respectively, relative to values measured after the initial rinses. All three decreases are significant (Student's t-test, two-tailed, p < 0.05). The Mg/Ca ratios decrease by 18% relative to values measured after the initial rinses, but this decrease is not significantly different (Student's t-test, two-tailed, p = 0.16).

Like *N. dutertrei*, few high TE bands remain in *P. obliquiloculata*, and shell thickness decreased by 20% (e.g., Figure 3, yellow lines). High TE calcite makes up just 15% of the total calcite, compared to 56% after the initial rinses/sonication. Ba/Ca, Mn/Ca, Zn/Ca, and Mg/Ca ratios decrease by 64%, 50%, 81%, and 26%, respectively, relative to values measured after the initial rinses. The decrease in Ba/Ca, Mn/Ca, and Zn/Ca ratios are statistically significant (Student's *t*-test, two-tailed, p < 0.05), while the decrease in Mg/Ca is not significant (Student's *t*-test, two-tailed, p = 0.06).







# (b) P. obliquiloculata

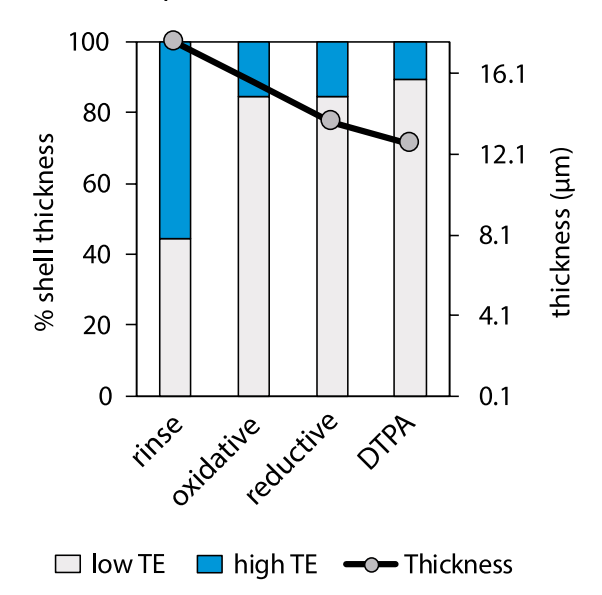


**Figure 4.** Shell thickness (μm; gray circles) and proportion of the shell thickness composed of low trace element (TE) outer calcite (gray bar) and high TE inner calcite (blue bar) after initial rinses (rinse), oxidative, reductive, and DTPA cleaning for *N. dutertrei* (a) and *P. obliquiloculata* (b) material. DTPA, diethylene-triamine pentaacetic acid.

# 3.2. DTPA cleaning

After the DTPA cleaning step, calcite with TE banding in N. dutertrei has been removed (e.g., Figure 2, purple lines). Shell thickness decreased by an average of 30% and high TE calcite comprises only 40% of the total calcite. Ba/Ca, Mn/Ca, Zn/Ca, and Mg/Ca ratios decrease by 82%, 49%, 91%, and 22%, respectively, relative to values measured after the initial rinses. The decrease in Ba/Ca, Mn/Ca, and Zn/Ca ratios are significant (Student's t-test, two-tailed, p < 0.01), and Mg/Ca ratios are not significantly different (Student's t-test, two-tailed, p = 0.07). In P. obliquioculata shells, nearly all calcite with high TE bands has been removed (e.g., Figure 3, purple lines). A few profiles contain only low TE ratio calcite, consistent with the removal of all inner calcite layers leaving behind only low TE cortex. The thickness of the shell wall decreases by 30% and high TE calcite make up just 10% of the total calcite. Ba/Ca, Mn/Ca, Zn/Ca and Mg/Ca ratios are reduced by 65%, 59%, 90%, and 19%, respectively, relative to values measured after the initial rinses. The decrease in Ba/Ca, Mn/Ca, and Zn/Ca ratios are significant (Student's t-test, two-tailed, p < 0.05), and Mg/Ca ratios are not significantly different (Student's t-test, two-tailed, p = 0.06).

In summary, shells progressively thin through chemical cleaning and high TE inner calcite is preferentially removed. We note that SEM analysis obtained before chemical cleaning indicate that EEP shells are well preserved, despite residing at a water depth of 1,368 m in waters with a  $\Delta(\text{CO}_3^{2-})$  of ~1–2 µmol/kg, ~500 m above the regional lysocline (~2,000 m water depth; GLODAP data set, Key et al., 2004). While dissolution may lower TE/Ca ratios in samples above the lysocline (Dekens et al., 2002; Regenberg et al., 2006), Mg/Ca Sea Surface Temperature (SST) estimates using the Anand et al. (2003) multispecies equation predict N. dutertrei and P. obliquiloculata calcified in 19.0°C and 19.5°C waters, consistent with these species depth habitat at the base of the thermocline (Elderfield & Ganssen, 2000; Farmer et al., 2007), further suggesting that dissolution did not significantly impact TE/Ca ratios in these specimens. SEM image analysis after cleaning reveals that in a few specimens, none of the high TE/Ca inner calcite remains. Chemical dissolution is evident from SEM analysis (widened pores, cracked surfaces, and delaminating shell structure) and shells are likely further agitated by handling and laser ablation. We note that shell fragmentation can occur during laser ablation analysis, often when the laser first strikes the shell surface unevenly (i.e., not perpendicular). Laser ablation is unlikely to be the main factor contributing to inner calcite loss, as uneven ablation results in large irregular pits, which we did not observe during our analyses. It is likely that both chemical and mechanical breakdown of the shell contribute to the loss of high TE/Ca inner calcite. Through the full cleaning process for single shells analyzed via laser ablation, Ba/Ca, Mn/Ca, and Zn/Ca values decrease by

 $\sim$  50%–90%. Mg/Ca ratios are not significantly affected throughout the cleaning process, likely because the Mg/Ca ratios are not markedly different in the inner versus outer calcite portions of the shell used in our study. Through the full cleaning process, Mg/Ca ratios decrease by 20%–25%, from 2.2 to 1.7 mmol/mol in *N. dutertrei* and 2.1 to 1.7 mmol/mol in *P. obliquiloculata* shells. This Mg/Ca decrease would translate to an Mg/Ca SST estimate of 19.0°C and 19.5°C, decreasing to 16.6°C. While the decrease in Mg/Ca is not significant, the Mg/Ca SST estimation suggests a lowering of several degrees that is likely an artifact of the cleaning process, as shells were initially observed to be well preserved, which is consistent with the reduction in Mg/Ca SST estimate observed by others (Martin & Lea, 2002; Regenberg et al., 2006; Rosenthal et al., 2004).



Table 2	
Mean and standard deviation (std dev. $1\sigma$ )	hrough individual shells of all individual shells before chemical cleaning

Species	Measurement	Ba/Ca (μmol/mol)		Mn/Ca (μmol/mol)		Zn/Ca (μmol/mol)		Mg/Ca (mmol/mol)	
		Mean	Std dev						
N. dutertrei	Whole shell	12.3	10.0	279.9	158.5	76.1	76.6	2.2	2.5
	High TE calcite	23.4	62.1	295.0	390.1	160.6	277.0	2.6	2.6
	Low TE calcite	1.6	0.8	102.2	54.2	39.9	41.8	1.7	0.5
P. obliquiloculata	Whole shell	10.7	10.6	218.0	105.3	102.7	73.9	2.1	2.1
	High TE calcite	13.0	37.1	250.0	386.5	168.0	91.3	2.1	2.1
	Low TE calcite	2.0	1.1	103.8	39.8	18.6	54.0	1.9	0.4

# 3.3. Bulk Shells

Bulk *P. obliquiloculata* were prepared for solution ICP-MS analysis by cracking the shells open and subjecting shells to initial rinses/sonication and an oxidative cleaning step. We compare the effect of using different sample cracking methods and settling times after rinses/sonication. We refer to the cleaning process with the standard crushing process (which yielded smaller fragments) and 1 min settling time after rapping the vials on the counter as the "traditional cleaning method." For the "careful cleaning method," the shells were cracked more gently such that the inside of shells were exposed while maximizing the size of shell fragments, and the amount of settling time after rapping the vials on the counter was increased from 1 to 3 min. The increased settling time was chosen to maximize the opportunity for small fragments to settle to the bottom of the vials before aspirating the rinse/cleaning solution.

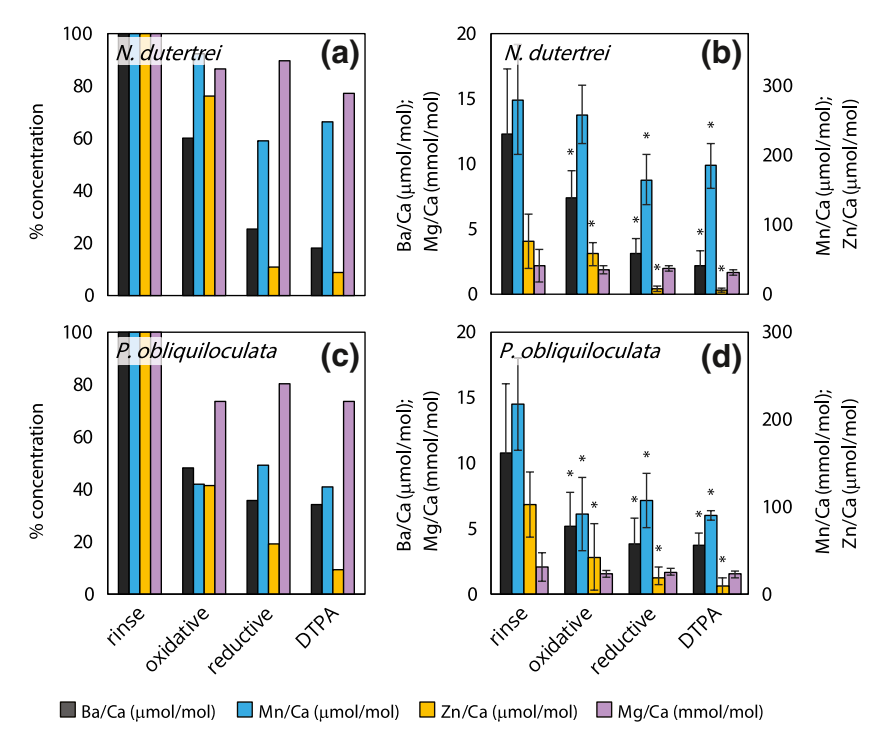


Figure 5. Laser ablation mean percent concentration of Ba/Ca ( $\mu$ mol/mol; gray bar), Mn/Ca ( $\mu$ mol/mol; blue bar), Zn/Ca (yellow bar;  $\mu$ mol/mol), and Mg/Ca (purple bar; mmol/mol) in *N. dutertrei* (a) and (b) and *P. obliquiloculata* (c) and (d) shell material after initial rinses (rinse), oxidative, reductive, and DTPA cleaning. Values are scaled to rinse measurements (a) and (c) and reported as mean and standard deviation (1 $\sigma$ ) (b) and (d). Star indicates a statistically significance difference from initial rinse values (Student's *t*-test, two-tailed). DTPA, diethylene-triamine pentaacetic acid.



Light microscope images were taken of bulk P. obliquiloculata fragments before and after cleaning and fragments were measured using image analysis techniques (Figures 2a-2c). We find that small shell fragments ( $<6 \,\mu\text{m}^2$ ) are preferentially removed during traditional cleaning (Figure S3). The proportion of small fragments is reduced by 3% in Holocene samples during traditional cleaning, which is not significant (Student's t-test, two-tailed, paired, p = 0.07). In deglacial samples, small fragments comprise 59% of the total calcite prior to traditional cleaning and comprise 28% after traditional cleaning steps, which is significantly different (Student's t-test, two-tailed, paired, p < 0.05). In contrast, when careful cleaning methods are used that include longer particle settling time, there is no significant difference in the number of small fragments before and after cleaning in Holocene samples (Student's t-test, two-tailed, paired, p = 0.26) nor in deglacial samples (Student's t-test, two-tailed, paired, p = 0.08). For all samples that underwent careful cleaning, more small fragments are retained than with traditional cleaning methods.

SEM images of the *P. obliquiloculata* fragments were taken after cleaning, and machine learning software was trained to categorize each pixel of the image as inner calcite or outer calcite (Figures 2d-2f). Holocene samples cleaned by traditional means retain 65% inner calcite, while when cleaned with careful procedures, Holocene samples retain 71% inner calcite, although the two groups are not significantly different (Student's *t*-test, two-tailed, paired, p = 0.29; Figure S4). Deglacial samples that underwent traditional cleaning steps retain just 25% inner calcite. In contrast, deglacial samples cleaned with careful procedures retain 70% inner calcite and are significantly different (Student's *t*-test, two-tailed, paired, p < 0.01).

# 4. Discussion

Ideally, geochemical measurements in planktic foraminifera yield the primary signal incorporated during calcification and can be used to interpret sea surface conditions. Our results demonstrate that N. dutertrei and P. obliquiloculata from the EEP have high TE/Ca ratios in the inner calcite with large intrashell TE variability (Figures 2 and 3; Table 2). Our TE/Ca measurements are higher and more variable compared to the range of values measured in surface dwelling species. These results are consistent with others that observed high and variable Ba/Ca, Mn/Ca, and Zn/Ca ratios in some deeper dwelling species compared to surface dwelling species (Eggins et al., 2003; Fehrenbacher et al., 2018; Hathorne et al., 2009; Kunioka et al., 2006; Steinhardt et al., 2015). In particular, the Ba/Ca ratios in our specimens are much higher than measurements in surface dwelling species, which are typically < 1-2 μmol/mol (Hall & Chan, 2004; Sprovieri et al., 2008; Weldeab et al., 2007a, b), and higher then values traditionally expected in planktic foraminifera (e.g., Lea & Boyle, 1991). However, few Ba/Ca, Mn/Ca, and Zn/Ca measurements have been made in deeper dwelling species and our results add to a growing collection that is needed to establish a range of expected values in foraminiferal species. High TE values—especially elevated Mg/Ca, Mn/Ca, and Ba/Ca—are traditionally attributed to non-lattice bound contaminants that should be removed before shell geochemistry can be accurately interpreted (Boyle, 1981, 1983; Boyle & Keigwin, 1985; Gibson et al., 2016; Haley & Klinkhammer, 2002; Lea & Boyle, 1989, 1990, 1991). We demonstrate that the efforts to remove shell contaminant phases with highly corrosive cleaning can also remove ontogenic calcite and lattice bound TEs.

Below, we first present the case that high TE values in our samples are lattice bound and are representative of conditions experienced by foraminifera during their ontogeny and argue against diagenesis governing the high TE values in our samples. We then describe the consequences of chemical and physical cleaning on inner calcite high in TEs and discuss implications for down core analysis. We use a simple mixing model to illustrate the consequences of over-cleaning shells. Finally, we provide suggestions for sample preparation and the careful interpretation of TE data in *N. dutertrei* and *P. obliquiloculata* and other deeper dwelling foraminifera that contain high intrashell TEs.

# 4.1. Biogenic Versus Abiotic High TE/Ca Ratios

In this study, TEs are high and most variable within *N. dutertrei* and *P. obliquiloculata* inner shell calcite. High intrashell variability is likely attributed to ontogenic incorporation of elevated TEs. Foraminifera grow by first forming relatively thinly calcified chambers during early adult stages before thickening with additions of outer calcite and sometimes an outer gametogenic crust or cortex that covers pre-existing ontogenic chambers (Fehrenbacher et al., 2017; Schiebel & Hemleben, 2017). Laser ablation profiles sample the entire



calcite wall and demonstrate clear transitions from inner calcite regions with elevated TEs and intra-shell TE variability to homogenous (and low) TE outer calcite. Our results corroborate earlier findings: high TE/Ca bands in deeper dwelling species are located within the inner part of the shell wall and may be associated with organic components linked to the early stages of shell growth (e.g., E. C. Hathorne et al., 2009; Kunioka et al., 2006), and possibly linked to early ontogenic growth in microhabitats (e.g., Fehrenbacher et al., 2018).

Aggressive cleaning procedures were established to remove contaminant phases (e.g., Lea & Boyle, 1991). Problematically, these procedures can remove primary calcite in addition to abiotic phases. For example, Lea and Boyle (1991) found high Ba/Ca ratios (up to 4.7 µmol/mol) in *N. dutertrei* shells from sediment traps that have never had contact with deep sea sediments, demonstrating the Ba in the shells was not a contaminant phase. Other researchers also clearly demonstrate elevated intrashell Ba and Mn in the species *Globorotalia inflata*, *Globorotalia scitula* (Hathorne et al., 2009) and *Globorotalia menardii* (Davis et al., 2020). While Lea and Boyle (1991) demonstrated that highly corrosive cleaning steps significantly lowered Ba/Ca ratios in *N. dutertrei*, they were never able to decrease the TE/Ca ratios as low as the Ba/Ca ratios of surface dwelling species and postulated that these measurements reflect a primary TE source in some deeper dwelling foraminifera.

Our analyses rule out the possibility that contamination is responsible for the elevated TE/Ca ratios in our samples. In laser ablation profiles, surface contaminant phases or reabsorption of contaminants during cleaning (Elderfield & Boyle, 1986; Klinkhammer et al., 2009) typically yield a spike in Al/Ca and Mn/Ca ratios on the inside and/or outside of the laser profile and these surface contaminants are excluded during data processing (e.g., Branson et al., 2019; Fehrenbacher et al., 2015). Average Ba/Ca and Zn/Ca ratios in our study do not correlate with Al/Ca nor Mn/Ca ratios and Mn/Ca ratios do not correlate with Mg/Ca ratios in N. dutertrei ( $R^2 < 0.05$ ) nor in P. obliquiloculata ( $R^2 < 0.05$ ; Figure S5). Additionally, there is no abrupt enrichment in Mn/Ca and Mg/Ca ratios at the innermost (Gibson et al., 2016; Pena et al., 2005, 2008) or outermost (Boyle, 1981) part of the shell that would indicate Mn-Mg rich oxide coating contamination. Mg/Ca and Mn/Ca measurements in this study in both N. dutertrei and P. obliquiloculata are also far lower than those observed by Pena et al. (2005),(2008; Mg/Ca ratios up to 6 mmol/mol and Mn/Ca ratios up to 25 mmol/mol in N. dutertrei). High TE/Ca ratios intrashell are likely not clay/contaminant infill in pore spaces because bands are consistent between laser profiles (Figures 2 and 3, solid and dashed blue lines), whereas contamination in pores would not be consistent from laser spot-to-spot. These rule out infill or metal overgrowths primarily controlling the high TE/Ca ratios observed in our shells. Finally, careful SEM observations rule out carbonate overgrowths or barite contamination governing high Ba/Ca ratios. We find no evidence of carbonate overgrowths that would appear under SEM as a layer of calcite precipitate on the shell surface, like those observed on a few EEP sediment trap (Gibson et al., 2016) and seafloor (Pena et al, 2005) foraminifera samples. The presence of barite crystals would appear under SEM as dense euhedral to subspherical crystals several microns on the longest axis, like those observed in core-top sediment from the EEP (Paytan et al., 2002) and within the shells of benthic foraminifera (Bertram & Cowen, 1997). SEM images of shell surfaces and inner-pore spaces taken after the initial rinses/sonication show no evidence of barite crystals under high magnification (<50 µm horizontal field width). This suggests that either barite crystals are not present in these samples or that they were removed with sonication in the initial rinses.

A biogenic origin of high TE inner calcite is supported by our microstructure analysis. Outer calcite appears as a smooth veneer with very fine tightly structured crystals and micropores in the case of *P. obliquiloculata* cortex (Figure 1l), or as larger blocky triangular prisms that often cover pore spaces in *N. dutertrei* crusts (Figure 1f). Outer calcite with this appearance is typically associated with a later foraminiferal life stage (Brown & Elderfield, 1996), and may be formed deeper in the water column or on the sea floor (Eggins et al., 2003; Fehrenbacher & Martin, 2010; Jonkers et al., 2012; Sautter, 1998; A. Y. Sadekov et al., 2005). The nature of the inner calcite in our study is compositionally distinct from observations of manganese carbonates or Mn-Fe oxides (see Figure 11 in Pena et al., 2005) and distinct from outer calcite cortex or crust. Inner calcite is composed of smaller and randomly oriented crystals and contains high irregular ridges between pore pits that appear in layers template over one another in cross section (Figure 1j). Laminations with radial calcite crystals laying perpendicular to the lamination are likely formed as a thin veneer of calcite is added to the pre-existing shell during ontogeny (Erez, 2003; Panieri et al., 2017), prior to the formation of the final chamber and the addition of outer calcite and final shell thickening (Fehrenbacher et al., 2017).

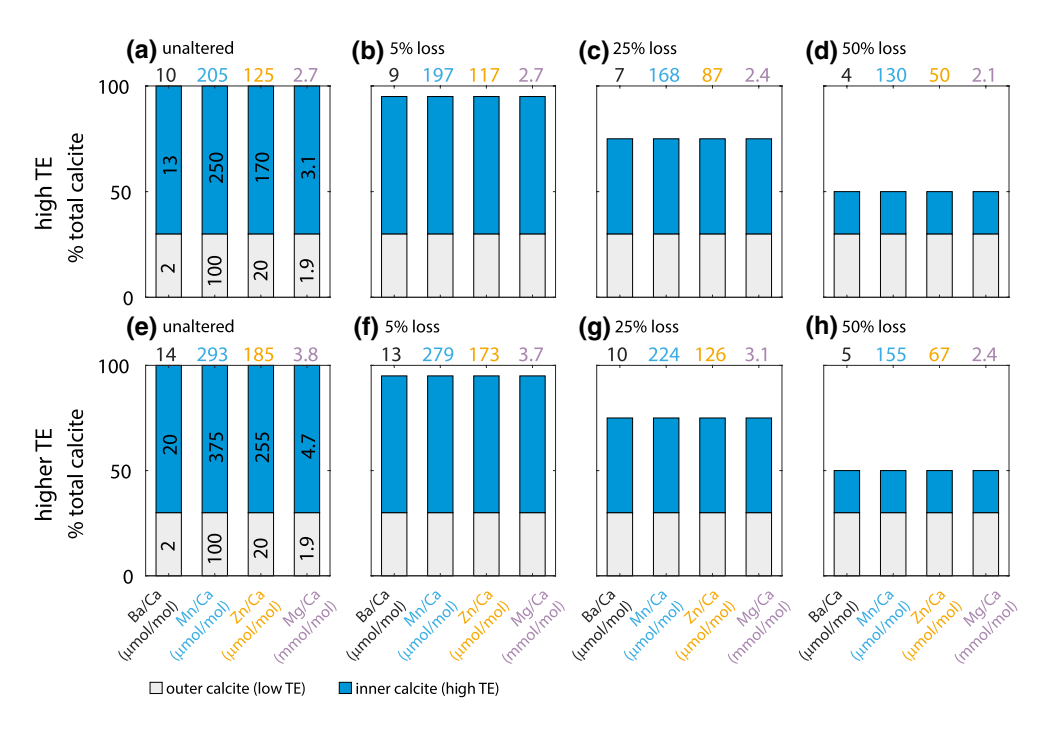


**Figure 6.** Simple mixing model results showing changing values when high TE inner calcite (a–d; inner and outer calcite Ba/Ca, Mn/Ca, Zn/Ca, and Mg/Ca concentrations in  $\mu$ mol/mol,  $\mu$ mol/mol,  $\mu$ mol/mol, and mmol/mol, respectively, overlay bar graph and calculated mean values are above each bar) is preferentially removed by 5% (b), 25% (c), and 50% (d) and higher TE inner calcite (e)–(h) is preferentially removed by 5% (f), 25% (g), and 50% (h).

# 4.2. Implications of Preferential Loss of High TE Inner Calcite during Solution Cleaning

We demonstrate that chemical and physical cleaning can preferentially remove inner calcite and significantly lower whole shell TE/Ca ratios. Because the inner calcite is enriched in some TEs relative to the outer calcite, the preferential loss of inner calcite has important implications for the interpretation of TE data. Here, we use a simple mixing model to demonstrate the effects of loss of high TE inner calcite. For the first model demonstration, we use mean P. obliquiloculata TE/Ca data obtained from the laser ablation analyses as the initial model parameters and estimate that the inner calcite represents  $\sim 70\%$  of the shell wall (e.g., Steinhardt et al., 2015). The following equation is used to calculate the mean TE/Ca:

$$\frac{\mathrm{TE}}{\mathrm{Ca}_{\mathrm{mean}}} = \left(f_1 * \frac{\mathrm{TE}}{\mathrm{Ca}_{\mathrm{inner}}}\right) + \left(f_2 * \frac{\mathrm{TE}}{\mathrm{Ca}_{\mathrm{outer}}}\right),$$

where TE/Ca<sub>mean</sub> is the mean TE/Ca value through the whole shell, TE/Ca<sub>inner</sub> is the mean of high TE calcite values from the inner calcite, TE/Ca<sub>outer</sub> is the mean of low TE calcite values from the outer calcite,  $f_1$  is the proportion of high TE inner calcite, and  $f_2$  is the proportion of low TE outer calcite. TE values used in the initial model demonstration (Ba/Ca, Mn/Ca, Zn/Ca, and Mg/Ca ratios for the inner and outer calcite) are summarized in Table 1 and shown in Figure 6a. To demonstrate the effect of inner calcite loss on mean TE/Ca values,  $f_1$  and  $f_2$  are scaled to simulate a decrease in inner calcite of 5%, which results in a decrease of mean Ba/Ca, Mn/Ca, and Zn/Ca ratios of 10%, 4%, and 6%, respectively, and a decrease in Mg/Ca ratios of 1%, which is less than 0.1 mmol/mol (Figure 6b). Conversely, a decrease in inner calcite of 25% results in a larger decrease of mean Ba/Ca, Mn/Ca, and Zn/Ca ratios (30%, 18%, and 30%, respectively) and a decrease in Mg/Ca ratios of just 11% or 0.3 mmol/mol (Figure 6c), and a decrease in inner calcite of 50% results in a decrease of mean Ba/Ca, Mn/Ca, and Zn/Ca ratios of 60%, 37%, and 60%, respectively, while average Mg/Ca ratios decrease of 22% or 0.6 mmol/mol (Figure 6d). A second demonstration illustrates the consequences of cleaning in shells with inner calcite with much higher TE/Ca ratios (50% higher, consistent with very high TE/Ca measurements made in inner calcite of P. obliquiloculata [e.g., Kunioka et al., 2006]). In this demonstration, a decrease in inner calcite of 5% results in a decrease of mean Ba/Ca, Mn/Ca, and Zn/Ca ratios of



8%, 5%, and 6%, respectively, and a loss of Mg/Ca of just 3% or 0.1 mmol/mol (Figure 6f). This decrease is modest; however, when more inner calcite is lost, consequences become severe. A decrease in inner calcite of 25% results in a decrease of mean Ba/Ca, Mn/Ca, and Zn/Ca ratios by 29%, 24%, and 31%, respectively (Figure 6g), and a decrease in Mg/Ca ratios of 26% or 0.7 mmol/mol, and a decrease in inner calcite of 50% results in a substantial decrease of mean Ba/Ca, Mn/Ca, and Zn/Ca ratios by 64%, 47%, and 64%, respectively, and a loss of Mg/Ca of 52% or 1.4 mmol/mol (Figure 6h).

This conceptual model, in which mean shell values are determined by the proportion of inner and outer calcite, in part, explains the drastic reduction in mean shell TE concentrations after traditional cleaning. When inner calcite high in TE is removed, more of the low TE outer calcite contributes to the whole shell mean, significantly decreasing the mean ratios of Ba/Ca, Mn/Ca, and Zn/Ca. Importantly, this simple mixing model also demonstrates why Mg/Ca ratios do not decrease as meaningfully as Ba/Ca, Mn/Ca, and Zn/Ca ratios, as the difference in Mg/Ca ratios between inner and outer calcite is not large enough to significantly alter mean Mg/Ca values when cleaning *P. obliquiloculata* shells. The model demonstrates that with much higher TEs in the inner calcite and substantial inner calcite loss (Figures 1g and 1h), cleaning does significantly impact mean Mg/Ca values.

The model also highlights the serious consequences of cleaning on downcore reconstructions. Traditional cleaning procedures remove a considerable portion of the inner calcite and decrease TE values significantly. However, when careful cleaning techniques are employed, less inner calcite is removed, and mean TE/Ca values are minimally impacted. Additionally, samples with very high inner calcite TE/Ca values can be highly impacted by inner calcite loss, while impacts are less important in samples with more uniform TE/ Ca values. This may have implications for comparing TE reconstructions between time periods/regions that have markedly higher inner calcite TE/Ca ratios to time periods/regions with lower TE/Ca inner calcite; the relative difference is dampened by the fact that samples with higher TE/Ca are more impacted by inner calcite loss. Additionally, dissolution caused by shells residing in bottom waters/pore waters that are undersaturated with respect to calcite may have similar effects to cleaning on TE/Ca ratios and may yield preferential dissolution of the inner calcite (Johnstone et al., 2010). In samples from undersaturated waters, TE/ Ca ratios may be dampened by both calcite dissolution in sediments and calcite dissolution during corrosive cleaning processes, particularly because samples that are already partly dissolved have weakened structures in inner calcite. Alternatively, in well-preserved shell from cores well above the regional lysocline, dissolution and cleaning may not as severely impact shell structure nor TE/Ca ratios, as compared to shells that have been impacted by dissolution in sediments. As the calcite saturation state is variable through time in cores close to the calcite saturation horizon, the dissolution effect on inner calcite may also vary through time in such locations.

# 4.3. Suggestions for Sample Preparation and TE Interpretation

No foraminifera cleaning technique is universally applicable, and few studies have addressed the effects of cleaning on the intrashell variability of Ba/Ca, Mn/Ca, and Zn/Ca ratios. We show that avoiding caustic chemicals during cleaning and/or using a "careful cleaning method" (with reduced shell cracking and increased settling times) of foraminifera shells retains more of the inner calcite high in TEs and preserves the primary TE/Ca signal incorporated during ontogeny. Furthermore, we demonstrate that elevated Ba/Ca, Mn/Ca, and Zn/Ca ratios are not always linked to diagenetic overprinting and in many cases aggressive cleaning steps are not necessary and remove fragile inner calcite and reduce the mean TE signal. The removal of the inner calcite is particularly problematic in samples where TE/Ca ratios in inner calcite are high, which likely varies from region-region and through time.

Sample cleaning for geochemical analysis should be based on the nature of the material and the TEs of interest, and care should be taken to determine if high Ba/Ca, Mn/Ca, and Zn/Ca are the result of contaminant phases or if they were incorporated during ontogeny before selecting cleaning methods for TE analysis. For accurate downcore reconstructions, we suggest the use of high-resolution techniques such as laser ablation and/or SEM analysis that first resolve the origin of high TEs (i.e., ontogenic vs. abiotic). If metal contaminants/precipitates are observed, or the material is suspected of high TE of abiotic origin, such as material originating from redox sensitive basins (e.g., Pena et al., 2005, 2008), the use of reductive chemicals may be appropriate (Panieri et al., 2017; Wan et al. 2018; Yu et al., 2007). If remnant organic material is suspected,



such as with material from recently living specimens or specimens from sediments with high organic matter content, the use of oxidative cleaning methods is recommended (e.g., Guo et al., 2019). The use of high-resolution sampling techniques (such as laser ablation depth profiling) in lieu of solution analyses could be employed for material of time slices of interest while still relying on bulk shell solution techniques for longer time-series reconstructions, considering that high-resolution techniques are costly and labor intensive. This would ensure that the contaminated portions of the shell wall are excluded (Gibson et al., 2016; Koho et al., 2015; Pena et al., 2008, 2005) without employing corrosive cleaning steps that could remove the primary TE/Ca signal. Furthermore, downcore reconstructions that relied on solution analysis and samples cleaned using corrosive cleaning steps may be reevaluated using high-resolution sampling techniques. Such techniques may lead to reinterpretations of previously published deeper dwelling foraminifera Ba/Ca, Mn/Ca, or Zn/Ca data as well as contributions of additional deeper dwelling foraminifera TE/Ca analysis which may increase the utility of Ba/Ca, Mn/Ca, and Zn/Ca in paleo-reconstructions.

# 5. Conclusion

We demonstrated, using the high-resolution sampling technique laser ablation ICP-MS, that deeper dwelling nonspinose foraminifera *N. dutertrei* and *P. obliquiloculata* have high and variable trace elements in the inner (ontogenic) calcite. We further demonstrate that chemical and mechanical cleaning preferentially removes the inner calcite in samples prepared for both single shell laser analyses and bulk solution analyses and favors the low trace element outer (crust/cortex) calcite. The preferential removal of inner calcite biases foraminiferal trace element results toward lower values and can yield data that is problematic for downcore applications. Mn/Ca, Ba/Ca, and Zn/Ca ratios, often very high in the ontogenic calcite and low in crust/cortex calcite, are particularly susceptible to alterations during cleaning, while Mg/Ca ratios are often more homogenous and less impacted. Careful evaluation of cleaning methods, incorporating laser ablation depth profiling, increases the potential for using trace elements such as Mn, Ba, and Zn in paleoclimate reconstructions. Furthermore, downcore reconstructions that relied on samples cleaned using the corrosive cleaning steps could be reevaluated using time-slice reconstructions and laser-ablation ICP-MS analyses.

# Appendix A: Summary of Individual Shell Cleaning

# A1. Step 1: Rinse

- Place each individual shell or shell fragment in a microcentrifuge vial.
- Rinse two to three times with methanol, ultrasonicating\* briefly (5–60 s in 5 s intervals).
- · Aspirate methanol. Before aspirating, rap rack or tap vials to remove air bubbles caught in chambers.
- Rinse three times in ultrapure water (18 M $\Omega$ ), ultrasonication\* briefly (5–30 s).
- · If shells appear unclean, repeat rinses above.

If clays remain, gently crack shells into larger fragments and repeat rinses without ultrasonication. Add ultrapure water "energetically" (i.e., squirt into bottom/sides of microcentrifuge vials so ultrapure water suspends loose clay particles/fragments). Allow fragments to settle before aspirations.

# A2. Step 2: Oxidative

- Prepare oxidative cleaning solution:  $100~\mu L$  of 9.8~M (30%)  $H_2O_2$  added to 30~mL of 0.1~M NaOH in fume hood.
- Add 100  $\mu L$  of the solution to individual microcentrifuge vials.
- Close vials and screw rack lid down to prevent vials from opening during the heating step.
- Place sample rack in warm water bath (~65°C) for 10 min, flip and briefly (5–30 s) ultrasonicate\* rack every 5 min.
- Allow samples to cool briefly (5 min), then rap rack to remove air bubbles caught in chambers.
- Aspirate solution, and rinse with ultrapure water four times (including vial caps); allow shells/fragments to settle to the bottom of the vial before aspirating water during rinses.



# A2. Step 3: Reductive

Step is not recommended unless metal oxide contaminants/Mn-Mg carbonate overgrowths are suspected/observed.

- Prepare reductive solution: mix 750  $\mu$ L of 31 M anhydrous hydrazine added to 10 mL of 0.25 M ammonium citrate and 10 mL of 14.6 M (30%) ammonium hydroxide in fume hood.
- Add 50 μL of solution to individual microcentrifuge vials.
- · Close vials and screw rack lid down to prevent vials from opening during the heating step.
- Place sample rack in sub-boiling (~90°C) water bath for 30 min, flip and briefly ultrasonicate\* (5 s) rack every 2–4 min.
- Allow to cool briefly (5 min), then rap rack to remove air bubbles caught in chambers.
- Aspirate solution, and rinse with ultrapure water four times (including vial caps); allow shells/fragments
  to settle to the bottom of the vial before aspirating water during rinses.

\*if observe shells fragmenting, stop ultrasonication. For Step 1, stop ultrasonication, skip rest of methanol rinses and proceed to ultrapure water rinses.

# **Data Availability Statement**

Data are available from https://doi.pangaea.de/10.1594/PANGAEA.922678.

### Acknowledgments:

MW91-9 6GGC core samples were obtained from Woods Hole Oceanographic Institute and ME0005A-43IC core samples from the Oregon State University (OSU) Marine and Geology Repository. The authors thank T. Sawyer and P. Eschbach of the OSU Electron Microscopy Facility for their assistance with SEM imaging and Chris Russo for his assistance on OSU's Keck Collaboratory laser ablation ICP-MS. Grace Meyer assisted with sample mounting on SEM pegs. Finally, we thank Catherine Davis whose feedback improved an earlier version of this manuscript. This work was supported by NSF MG&G Award OCE-1737165.

# References

Alldredge, A. L. (2000). Interstitial dissolved organic carbon (DOC) concentrations within sinking marine aggregates and their potential contribution to carbon flux. Limnology & Oceanography, 45, 1245–1253. https://doi.org/10.4319/lo.2000.45.6.1245

Alldredge, A. L., & Cohen, Y. (1987). Can microscale chemical patches persist in the sea - microelectrode study of marine snow, fecal pellets. *Science*, 235, 689–691.

Anand, P., Elderfield, H., & Conte, M. H. (2003). Calibration of Mg/Ca thermometry in planktonic foraminifera from a sediment trap time series. *Paleoceanography*, 18(2), 1050. https://doi.org/10.1029/2002PA000846

Bahr, A., Schönfeld, J., Hoffmann, J., Voigt, S., Aurahs, R., Kucera, M., & Gerdes, A. (2013). Comparison of Ba/Ca and δ<sup>18</sup>O<sub>WATER</sub> as freshwater proxies: A multi-species core-top study on planktonic foraminifera from the vicinity of the Orinoco River mouth. *Earth and Planetary Science Letters*, 383, 45–57. https://doi.org/10.1016/j.epsl.2013.09.036

Barker, S., Greaves, M., & Elderfield, H. (2003). A study of cleaning procedures used for foraminiferal Mg/Ca paleothermometry. *Geochemistry, Geophysics, Geosystems*, 4(9), 1–20. https://doi.org/10.1029/2003GC000559

Bertram, M. A., & Cowen, J. P. (1997). Morphological and compositional evidence for biotic precipitation of marine barite. *Journal of Marine Research*, 55, 577–593. https://doi.org/10.1357/0022240973224292

Boyle, E. A. (1981). Cadmium, zinc, copper, and barium in foraminifera tests. Earth and Planetary Science Letters, 53(1), 11–35.

 $Boyle, E.\ A.\ (1983).\ Manganese\ carbonate\ overgrowths\ on\ for a minifera\ tests.\ \textit{Geochimica}\ et\ \textit{Cosmochimica}\ Acta,\ 47(10),\ 1815-1819.$ 

Boyle, E. A., & Keigwin, L. D. (1985). Comparison of Atlantic and Pacific paleochemical records for the last 215,000 years: Changes in deep ocean circulation and chemical inventories. *Earth and Planetary Science Letters*, 76(1–2), 135–150.

Branson, O., Fehrenbacher, J. S., Vetter, L., Sadekov, A. Y., Eggins, S. M., & Spero, H. J. (2019). LAtools: A data analysis package for the reproducible reduction of LA-ICPMS data. *Chemical Geology*, 504, 83–95. https://doi.org/10.1016/j.chemgeo.2018.10.029

Branson, O., Read, E., Redfern, S. A., Rau, C., & Elderfield, H. (2015). Revisiting diagenesis on the Ontong Java Plateau: Evidence for authigenic crust precipitation in Globorotalia tumida. *Paleoceanography*, 30(11), 1490–1502. https://doi.org/10.1002/2014PA002759

Brown, S. J., & Elderfield, H. (1996). Variations in Mg/Ca and Sr/Ca ratios of planktonic foraminifera caused by post depositional dissolution: Evidence of shallow Mg-dependent dissolution. *Paleoceanography*, 11(5), 543–551. https://doi.org/10.1029/96PA01491

Bryan, S. P., & Marchitto, T. M. (2010). Testing the utility of paleonutrient proxies Cd/Ca and Zn/Ca in benthic foraminifera from thermocline waters. *Geochemistry, Geophysics, Geosystems*, 11(1), Q01005. https://doi.org/10.1029/2009GC002780

Chaisson, W. P., & Ravelo, A. C. (2000). Pliocene development of the east-west hydrographic gradient in the equatorial Pacific. *Paleocean-ography*, 15(5), 497–505. https://doi.org/10.1029/1999PA000442

Davis, C. V., & Benitez-Nelson, C. R. (2020). Evidence for rapid trace element alteration of planktic foraminiferal shells from the Panama Basin: Manganese adsorption during vertical transport. *Marine Micropaleontology*, 157, 101872. https://doi.org/10.1016/j.marmicro.2020.101872

Davis, C. V., Fehrenbacher, J. S., Benitez-Nelson, C. R., & Thunell, R. (2020). Trace element heterogeneity across individual planktic foraminifera from the Modern Cariaco Basin. *Journal of Foraminiferal Research*, 50(2), 204–218. https://doi.org/10.2113/gsjfr.50.2.204

Dekens, P. S., Lea, D. W., Pak, D. K., & Spero, H. J. (2002). Core top calibration of Mg/Ca in tropical foraminifera: Refining paleotemperature estimation. *Geochemistry, Geophysics, Geosystems*, 3(4), 1–29. https://doi.org/10.1029/2001GC000200

Dittert, N., & Henrich, R. (2000). Carbonate dissolution in the South Atlantic ocean: Evidence from ultrastructure breakdown in Globigerina bulloides. *Deep Sea Research Part I: Oceanographic Research Papers*, 47(4), 603–620. https://doi.org/10.1016/S0967-0637(99)00069-2 Edmond, J. M., Boyle, E. D., Drummond, D., Grant, B., & Mislick, T. (1978). *Netherlands Journal of Sea Research*, 12, 324.

Eggins, S., De Deckker, P., & Marshall, J. (2003). Mg/Ca variation in planktonic foraminifera tests: Implications for reconstructing paleoseawater temperature and habitat migration. *Earth and Planetary Science Letters*, 212(3–4), 291–306. https://doi.org/10.1016/s0012-821x(03)00283-8



- Elderfield, H., & Boyle, E. (1986). Rare earth elements in the shells of benthic foraminifera. Eos, 67, 1064.
- Elderfield, H., & Ganssen, G. (2000). Past temperature and  $\delta^{18}$ O of surface ocean waters inferred from foraminiferal Mg/Ca ratios. *Nature*, 405(6785), 442–445. https://doi.org/10.1038/35013033
- Erez, J. (2003). The source of ions for biomineralization in foraminifera and their implications for paleoceanographic proxies. *Reviews in Mineralogy and Geochemistry*, 54(1), 115–149. https://doi.org/10.2113/0540115
- Evans, D., Erez, J., Oron, S., & Müller, W. (2015). Mg/Ca-temperature and seawater-test chemistry relationships in the shallow-dwelling large benthic foraminifera Operculina ammonoides. *Geochimica et Cosmochimica Acta*, 148, 325–342. https://doi.org/10.1002/2015GC005822
- Farmer, E. C., Kaplan, A., de Menocal, P. B., & Lynch-Stieglitz, J. (2007). Corroborating ecological depth preferences of planktonic foraminifera in the tropical Atlantic with the stable oxygen isotope ratios of core top specimens. *Paleoceanography*, 22(3), PA3205. https://doi.org/10.1029/2006PA001361
- Fehrenbacher, J. S., & Martin, P. A. (2010). A comparison of intrashell Mg/Ca variability of the planktonic foraminifera G. ruber, G. sacculifer, and N. dutertrei determined by electron microprobe image mapping, 2010 IOP Conference Series. *Earth and Environmental Science*, 9. https://doi.org/10.1088/1755-1315/9/1/012018
- Fehrenbacher, J. S., Russell, A. D., Davis, C. V., Gagnon, A. C., Spero, H. J., Cliff, J. B., & Martin, P. (2017). Link between light-triggered Mg-banding and chamber formation in the planktic foraminifera Neogloboquadrina dutertrei. *Nature Communications*, 8(1), 1–10. https://doi.org/10.1038/ncomms15441
- Fehrenbacher, J. S., Russell, A. D., Davis, C. V., Spero, H. J., Chu, E., & Hönisch, B. (2018). Ba/Ca ratios in the non-spinose planktic foraminifer Neogloboquadrina dutertrei: Evidence for an organic aggregate microhabitat. *Geochimica et Cosmochimica Acta*, 236, 361–372. https://doi.org/10.1016/j.gca.2018.03.008
- Fehrenbacher, J. S., Spero, H. J., Russell, A. D., Vetter, L., & Eggins, S. (2015). Optimizing LA-ICP-MS analytical procedures for elemental depth profiling of foraminifera shells. *Chemical Geology*, 407, 2–9. https://doi.org/10.1015/j.chemgeol.2014.04.007
- Gibson, K. A., Thunell, R. C., Machain-Castillo, M. L., Fehrenbacher, J., Spero, H. J., Wejnert, K., & Tappa, E. J. (2016). Evaluating controls on planktonic foraminiferal geochemistry in the Eastern Tropical North Pacific. *Earth and Planetary Science Letters*, 452, 90–103. https://doi.org/10.1016/j.epsl.2016.07.039
- Glock, N., Eisenhauer, A., Liebetrau, V., Wiedenbeck, M., Hensen, C., & Nehrke, G. (2012). EMP and SIMS studies on Mn/Ca and Fe/Ca systematics in benthic foraminifera from the Peruvian OMZ: A contribution to the identification of potential redox proxies and the impact of cleaning protocols. *Biogeosciences*, 9(1), 341–359. https://doi.org/10.5194/bg-9-341-2012
- Greco, M., Jonkers, L., Kretschmer, K., Bijma, J., & Kucera, M. (2019). Depth habitat of the planktonic foraminifera Neogloboquadrina pachyderma in the northern high latitudes explained by sea-ice and chlorophyll concentrations. *Biogeosciences*, 16(17), 3425–3437. https://doi.org/10.5194/bg-16-3425-2019
- Groeneveld, J., Filipsson, H. L., Austin, W. E., Darling, K., McCarthy, D., Krupinski, N. B. Q., & Schweizer, M. (2018). Assessing proxy signatures of temperature, salinity, and hypoxia in the Baltic Sea through foraminifera-based geochemistry and faunal assemblages. *Journal of Micropalaeontology*, 37(2), 403–429. https://doi.org/10.5194/jm-37-403-2018
- Guo, X., Xu, B., Burnett, W. C., Yu, Z., Yang, S., Huang, X., & Sun, F. (2019). A potential proxy for seasonal hypoxia: LA-ICP-MS Mn/Ca ratios in benthic foraminifera from the Yangtze River Estuary. *Geochimica et Cosmochimica Acta*, 245, 290–303. https://doi.org/10.1016/j.gca.2018.11.007
- Haley, B. A., & Klinkhammer, G. P. (2002). Development of a flow-through system for cleaning and dissolving foraminiferal tests. *Chemical Geology*, 185(1–2), 51–69. https://doi.org/10.1016/S0009-2541(01)00399-0
- Hall, J. M., & Chan, L. H. (2004). Ba/Ca in Neogloboquadrina pachyderma as an indicator of deglacial meltwater discharge into the western Arctic Ocean. *Paleoceanography*, 19, PA1017. https://doi.org/10.1029/2003PA000910
- Hathorne, E. C., Alard, O., James, R. H., & Rogers, N. W. (2003). Determination of intra-test variability of trace elements in foraminifera by laser ablation inductively coupled plasma mass spectrometry. *Geochemistry, Geophysics, Geosystems*, 4(12), 14. https://doi.org/10.1029/2003GC000539
- Hathorne, E. C., James, R. H., & Lampitt, R. S. (2009). Environmental versus biomineralization controls on the intratest variation in the trace element composition of the planktonic foraminifera G. inflata and G. scitula. *Paleoceanography*, 24(4), PA4204. https://doi.org/10.1029/2009PA001742
- Hoffmann, J., Bahr, A., Voigt, S., Schönfeld, J., Nürnberg, D., & Rethemeyer, J. (2014). Disentangling abrupt deglacial hydrological changes in northern South America: Insolation versus oceanic forcing. Geology, 42(7), 579–582. https://doi.org/10.1130/G35562.1
- Jochum, K. P., Weis, U., Stoll, B., Kuzmin, D., Yang, Q., Raczek, I., & Günther, D. (2011). Determination of reference values for NIST SRM 610–617 glasses following ISO guidelines. *Geostandards and Geoanalytical Research*, 35(4), 397–429. https://doi.org/10.1111/j.1751-908X.2011.00120.x
- Johnstone, H. J., Lee, W., & Schulz, M. (2016). Effect of preservation state of planktonic foraminifera tests on the decrease in Mg/Ca due to reductive cleaning and on sample loss during cleaning. *Chemical Geology*, 420, 23–36. https://doi.org/10.1016/j.chemgeo.2015.10.045
- Johnstone, H. J., Schulz, M., Barker, S., & Elderfield, H. (2010). Inside story: An X-ray computed tomography method for assessing dissolution in the tests of planktonic foraminifera. *Marine Micropaleontology*, 77(1–2), 58–70. https://doi.org/10.1016/j.marmicro.2010.07.004
- Jonkers, L., Buse, B., Brummer, G. J. A., & Hall, I. R. (2016). Chamber formation leads to Mg/Ca banding in the planktonic foraminifer Neogloboquadrina pachyderma. Earth and Planetary Science Letters, 451, 177–184. https://doi.org/10.1016/j.epsl.2016.07.030
- Jonkers, L., De Nooijer, L. J., Reichart, G. J., Zahn, R., & Brummer, G. J. (2012). Encrustation and trace element composition of Neogloboquadrina dutertrei assessed from single chamber analyses implications for paleotemperature estimates. *Biogeosciences*, 9(11), 4851–4860. https://doi.org/10.5194/bg-9-4851-2012
- Key, R. M., Kozyr, A., Sabine, C. L., Lee, K., Wanninkhof, R., Bullister, J. L., & Peng, T. H. (2004). A global ocean carbon climatology: Results from Global Data Analysis Project (GLODAP). Global Biogeochemical Cycles, 18(4), GB4031. https://doi.org/10.1029/2004GB002247
- Kitano, Y., Kanamori, N., & Oomori, T. (1971). Measurements of distribution coefficients and barium between carbonate precipitate—Abnormally high values of distribution measured at early stages of carbonate of strontium and solution coefficients formation. *Geochemical Journal*, 4(4), 183–206
- Klinkhammer, G. P., Mix, A. C., & Haley, B. A. (2009). Increased dissolved terrestrial input to the coastal ocean during the last deglaciation. Geochemistry, Geophysics, Geosystems, 10(3), Q03009. https://doi.org/10.1029/2008GC002219
- Koho, K. A., de Nooijer, L. J., & Reichart, G. J. (2015). Combining benthic foraminiferal ecology and shell Mn/Ca to deconvolve past bottom water oxygenation and paleoproductivity. *Geochimica et Cosmochimica Acta*, 165, 294–306. https://doi.org/10.1016/j.gca.2015.06.003
- Kunioka, D., Shirai, K., Takahata, N., Sano, Y., Toyofuku, T., & Ujiie, Y. (2006). Microdistribution of Mg/Ca, Sr/Ca, and Ba/Ca ratios in Pulleniatina obliquiloculata test by using a NanoSIMS: Implication for the vital effect mechanism. *Geochemistry, Geophysics, Geosystems*, 7(12), Q12P20. https://doi.org/10.1029/2006GC001280



- Lea, D., & Boyle, E. (1989). Barium content of benthic foraminifera controlled by bottom-water composition. *Nature*, 338(6218), 751–753.
  Lea, D. W., & Boyle, E. A. (1990). Foraminiferal reconstruction of barium distributions in water masses of the glacial oceans. *Paleocean-ography*, 5(5), 719–742.
- Lea, D. W., & Boyle, E. A. (1991). Barium in planktonic foraminifera. Geochimica et Cosmochimica Acta, 55(11), 3321-3331.
- Lea, D. W., Mashiotta, T. A., & Spero, H. J. (1999). Controls on magnesium and strontium uptake in planktonic foraminifera determined by live culturing. *Geochimica et Cosmochimica Acta*, 63(16), 2369–2379. https://doi.org/10.1016/S0016-7037(99)00197-0
- Lea, D. W., & Spero, H. J. (1994). Assessing the reliability of paleochemical tracers—Barium uptake in the shells of planktonic foraminifera. *Paleoceanography*, 9, 445–45.
- Marchitto, T. M., Jr, Curry, W. B., & Oppo, D. W. (2000). Zinc concentrations in benthic foraminifera reflect seawater chemistry. *Paleocean-ography*, 15(3), 299–306. https://doi.org/10.1029/1999PA000420
- Marr, J. P., Carter, L., Bostock, H. C., Bolton, A., & Smith, E. (2013). Southwest Pacific Ocean response to a warming world: Using Mg/Ca, Zn/Ca, and Mn/Ca in foraminifera to track surface ocean water masses during the last deglaciation. *Paleoceanography*, 28(2), 347–362.
- Martinez-Ruiz, F., Jroundi, F., Paytan, A., Guerra-Tschuschke, I., del Mar Abad, M., & González Muñoz, M. T. (2018). Barium bioaccumulation by bacterial biofilms and implications for Ba cycling and use of Ba proxies. *Nature Communications*, 9(1), 1–9. https://doi.org/10.1038/s41467-018-04069-z
- Martin, P. A., & Lea, D. W. (2002). A simple evaluation of cleaning procedures on fossil benthic foraminiferal Mg/Ca. *Geochemistry, Geophysics, Geosystems*, 3(10), 1–8. https://doi.org/10.1029/2001GC000280
- Monnin, C., Jeandel, C., Cattaldo, T., & Dehairs, F. (1999). The marine barite saturation state of the world's oceans. *Marine Chemistry*, 65, 253–261.
- Mulitza, S., Dürkoop, A., Hale, W., Wefer, G., & Stefan Niebler, H. (1997). Planktonic foraminifera as recorders of past surface-water stratification. *Geology*, 25(4), 335–338. https://doi.org/10.1130/00917613(1997)025<0335:PFAROP>2.3.CO;2
- Panieri, G., Lepland, A., Whitehouse, M. J., Wirth, R., Raanes, M. P., James, R. H., & Schneider, A. (2017). Diagenetic Mg-calcite overgrowths on foraminiferal tests in the vicinity of methane seeps. *Earth and Planetary Science Letters*, 458, 203–212. https://doi.org/10.1016/j.epsl.2016.10.024
- Paytan, A., Mearon, S., Cobb, K., & Kastner, M. (2002). Origin of marine barite deposits: Sr and S isotope characterization. *Geology*, 30, 747–750. https://doi.org/10.1130/0091-7613(2002)030<0747:OOMBDS>2.0.CO;2
- Pedersen, T. F., & Price, N. B. (1982). The geochemistry of manganese carbonate in Panama Basin sediments. *Geochimica et Cosmochimica Acta*, 46, 69–74.
- Pena, L. D., Cacho, I., Calvo, E., Pelejero, C., Eggins, S., & Sadekov, A. (2008). Characterization of contaminant phases in foraminifera carbonates by electron microprobe mapping. *Geochemistry, Geophysics, Geosystems*, 9(7), Q07012. https://doi.org/10.1029/2008GC002018
- Pena, L. D., Calvo, E., Cacho, I., Eggins, S., & Pelejero, C. (2005). Identification and removal of Mn Mg rich contaminant phases on foraminiferal tests: Implications for Mg/Ca past temperature reconstructions. *Geochemistry, Geophysics, Geosystems*, 6(9), Q09P02. https://doi.org/10.1029/2005GC000930
- Petersen, J., Barras, C., Bézos, A., La, C., Slomp, C. P., Meysman, F. J., et al. (2019). Mn/Ca ratios of Ammonia tepida as a proxy for seasonal coastal hypoxia. *Chemical Geology*, 518, 55–66. https://doi.org/10.1016/j.chemgeo.2019.04.002
- Regenberg, M., Nürnberg, D., Steph, S., Groeneveld, J., Garbe-Schönberg, D., Tiedemann, R., & Dullo, W. C. (2006). Assessing the effect of dissolution on planktonic foraminiferal Mg/Ca ratios: Evidence from Caribbean core tops. *Geochemistry, Geophysics, Geosystems*, 7(7), 007P15. https://doi.org/10.1029/2005GC001019
- Regenberg, M., Schröder, J. F., Jonas, A. S., Woop, C., & Gorski, L. (2013). Weight loss and elimination of planktonic foraminiferal tests in a dissolution experiment. *The Journal of Foraminiferal Research*, 43(4), 406–414. https://doi.org/10.2113/gsjfr.43.4.406
- Rosenthal, Y., Perron-Cashman, S., Lear, C. H., Bard, E., Barker, S., Billups, K., & Elderfield, H. (2004). Interlaboratory comparison study of Mg/Ca and Sr/Ca measurements in planktonic foraminifera for paleoceanographic research. *Geochemistry, Geophysics, Geosystems*, 5(4). https://doi.org/10.1029/2003GC000650
- Rushdi, A. I., McManus, J., & Collier, R. W. (2000). Marine barite and celestite saturation in seawater. *Marine Chemistry*, 69, 19–31. https://doi.org/10.1016/S0304-4203(99)00089-4
- Sadekov, A. Y., Eggins, S. M., & De Deckker, P. (2005). Characterization of Mg/Ca distributions in planktonic foraminifera species by electron microprobe mapping. *Geochemistry, Geophysics, Geosystems*, 6(12), Q12P06. https://doi.org/10.1029/2005GC000973
- Sadekov, A., Eggins, S. M., De Deckker, P., Ninnemann, U., Kuhnt, W., & Bassinot, F. (2009). Surface and subsurface seawater temperature reconstruction using Mg/Ca microanalysis of planktonic foraminifera Globigerinoides ruber, Globigerinoides sacculifer, and Pulleniatina obliquiloculata. *Paleoceanography*, 24(3), 17. https://doi.org/10.1029/2008PA001664
- Sautter, L. R. (1998). Morphologic and stable isotopic variability within the planktic foraminiferal genus Neogloboquadrina. *The Journal of Foraminiferal Research*, 28(3), 220–232.
- Schiebel, R., & Hemleben, C. (2017). Planktic foraminifers in the modern ocean. (p. 1–358). Berlin: Springer.
- Schindelin, J., Arganda-Carreras, I., & Frise, E. (2012). Fiji: an open-source platform for biological image analysis. *Nature Methods*, 9(7), 676–682. https://doi.org/10.1038/nmeth.2019
- Setiawan, R. Y., Wirasatriya, A., Shaari, H. B., Setyobudi, E., & Rachman, F. (2017). Assessing the reliability of Planktic Foraminifera Ba/Ca as a proxy for salinity off the Sunda Strait. *International Journal of Marine Science*, 22(4), 201–212.
- Sholkovitz, E. R. (1989). Artifacts associated with the chemical leaching of sediments for rare-earth elements. *Chemical Geology*, 77(1), 47–51.
- Skinner, L. C., Sadekov, A., Brandon, M., Greaves, M., Plancherel, Y., de La Fuente, M., & Scrivner, A. E. (2019). Rare Earth Elements in early-diagenetic foraminifer 'coatings': Pore-water controls and potential paleoceanographic applications. *Geochimica et Cosmochimica Acta*, 245, 118–132. https://doi.org/10.1016/j.gca.2018.10.027
- Spero, H. J., Mielke, K. M., Kalve, E. M., Lea, D. W., & Pak, D. K. (2003). Multispecies approach to reconstructing eastern equatorial Pacific thermocline hydrography during the past 360 kyr. *Paleoceanography*, 18(1), 1022. https://doi.org/10.1029/2002PA000814
- Sprovieri, M., d'Alcalà, M. R., Manta, D. S., Bellanca, A., Neri, R., Lirer, F., & Sammartino, S. (2008). Ba/Ca evolution in water masses of the Mediterranean late Neogene. *Paleoceanography*, 23(3), 17. https://doi.org/10.1029/2007PA001469
- Steinhardt, J., de Nooijer, L. L., Brummer, G. J., & Reichart, G. J. (2015). Profiling planktonic foraminiferal crust formation. *Geochemistry*, *Geophysics, Geosystems*, 16(7), 2409–2430. https://doi.org/10.1002/2015GC005752
- Sternberg, E., Tang, D., Ho, T. Y., Jeandel, C., & Morel, F. M. (2005). Barium uptake and adsorption in diatoms. Geochimica et Cosmochimica Acta, 69(11), 2745–2752. https://doi.org/10.1016/j.gca.2004.11.026
- Stroobants, N., Dehairs, F., Goeyens, L., Vanderheijden, N., & Vangrieken, R. (1991). Barite formation in the southern-ocean water column. Marine Chemistry, 35, 411–421.



- Takagi, H., Kimoto, K., Fujiki, T., Saito, H., Schmidt, C., Kucera, M., & Moriya, K. (2019). Characterizing photosymbiosis in modern planktonic foraminifera. *Biogeosciences*, 16(17), 1–32. https://doi.org/10.5194/bg-16-3377-2019
- Vetter, L., Spero, H. J., Russell, A. D., & Fehrenbacher, J. S. (2013). LA-ICP-MS depth profiling perspective on cleaning protocols for elemental analyses in planktic foraminifers. *Geochemistry, Geophysics, Geosystems*, 14, 2916–2931. https://doi.org/10.1002/ggge.20163
- von Langen, P. J., Pak, D. K., Spero, H. J., & Lea, D. W. (2005). Effects of temperature on Mg/Ca inneogloboquadrinid shells determined by live culturing. *Geochemistry, Geophysics, Geosystems*, 6, Q10P03. https://doi.org/10.1029/2005GC000989
- Wan, S., Feng, D., Chen, F., Zhuang, C., & Chen, D. (2018). Foraminifera from gas hydrate-bearing sediments of the northeastern South China Sea: Proxy evaluation and application for methane release activity. *Journal of Asian Earth Sciences*, 168, 125–136. https://doi.org/10.1016/j.jseaes.2018.04.036
- Weldeab, S., Lea, D. W., Oberhänsli, H., & Schneider, R. R. (2014). Links between southwestern tropical Indian Ocean SST and precipitation over southeastern Africa over the last 17 kyr. *Palaeogeography, palaeoclimatology, palaeoecology, 410*, 200–212. https://doi.org/10.1016/j.palaeo.2014.06.001
- Weldeab, S., Lea, D. W., Schneider, R. R., & Andersen, N. (2007a). 155,000 years of west African monsoon and ocean thermal evolution. Science, 316, 1303–1307. https://doi.org/10.1126/science.1140461
- Weldeab, S., Lea, D. W., Schneider, R. R., & Andersen, N. (2007b). Centennial scale climate instabilities in a wet early Holocene West African monsoon. *Geophysical Research Letters*, 34, L24702. https://doi.org/10.1029/2007GL031898
- Wit, J. C., Reichart, G. J., A Jung, S. J., & Kroon, D. (2010). Approaches to unravel seasonality in sea surface temperatures using paired single-specimen foraminiferal  $\delta^{18}$ O and Mg/Ca analyses. *Paleoceanography*, 25(4), PA4220. https://doi.org/10.1029/2009PA001857
- Yu, J., Elderfield, H., Greaves, M., & Day, J. (2007). Preferential dissolution of benthic foraminiferal calcite during laboratory reductive cleaning. *Geochemistry, Geophysics, Geosystems*, 8(6), Q06016. https://doi.org/10.1029/2006GC001571